

N 64 32996
 (ACCESSION NUMBER)
 31
 (PAGES)
 CR-59183
 (NAX CR OR TX OR AD NUMBER)

(THRU)
 1
 (CODE)
 23
 (CATEGORY)

Technical Report No. 32-646

A Fiber Optical System for Space Application

Robert Y. Wong

OTS PRICE

XEROX \$ 2.00 FS
 MICROFILM \$ 0.50 mfi



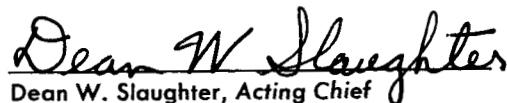
JET PROPULSION LABORATORY
CALIFORNIA INSTITUTE OF TECHNOLOGY
PASADENA, CALIFORNIA

August 31, 1964

Technical Report No. 32-646

A Fiber Optical System for Space Application

Robert Y. Wong


Dean W. Slaughter, Acting Chief
Space Instrument Systems Section

JET PROPULSION LABORATORY
CALIFORNIA INSTITUTE OF TECHNOLOGY
PASADENA, CALIFORNIA

August 31, 1964

**Copyright © 1964
Jet Propulsion Laboratory
California Institute of Technology**

**Prepared Under Contract No. NAS 7-100
National Aeronautics & Space Administration**

CONTENTS

I. Introduction	3
II. Fiber Optics	3
A. General Characteristics	3
B. Analysis of Transmission Efficiency	5
C. Analysis of Contrast and Resolution	9
D. Analysis of Fiber Optical Cone	12
E. Application of Fresnel Lens	13
III. Fiber Optical System Design	14
A. Optical System Requirements	14
B. Design of Fiber Optical Cone	14
C. Design of Fresnel Lens	16
D. Design of Fiber Optical System	17
IV. Fiber Optical System Fabrication	18
A. Fabrication of Image-Forming Lens	18
B. Fabrication of Fiber Optical Cone	19
C. Fabrication of Fresnel Lens	19
D. Construction of Fiber Optical System	20
V. System Performance Evaluation	22
A. Image-Forming Lens Tests	22
B. Fiber Optical System Tests	23
VI. Discussion and Conclusions	24
References	25

TABLE

1. Ratio of transmitted energy to leakage energy for the primary refraction ray through fibers with $N_0 = 1.00$, $N_1 = 1.80$, $N_2 = 1.50$ and $\theta_0 = 8$ deg	11
---	----

FIGURES

1. Numerical aperture as a function of N_1/N_2	3
2. Cylindrical fiber	5

FIGURES (Cont'd)

3. Transmission efficiency as a function of incident light angle due to surface-reflection losses	6
4. Transmission efficiency as a function of AL due to glass-absorption loss	6
5. Transmission efficiency as a function of half angle of incident light cone for $d = 10 \mu$	7
6. Transmission efficiency as a function of half angle of incident light cone for $d = 25 \mu$	8
7. Transmission efficiency as a function of half angle of incident light cone for $d = 50 \mu$	8
8. Transmission efficiency as a function of fiber length	8
9. Transmission efficiency as a function of fiber diameter	8
10. Regions of leakage concentration	9
11. Leakage due to internal reflection	9
12. Light leakage as a function of half angle of incident cone, $d = 10 \mu$	11
13. Light leakage as a function of half angle of incident cone, $d = 25, 50 \mu$	11
14. Fiber optical cone	12
15. Lens system and fiber cone	13
16. Fresnel lens (a) the lens (b) an element of the lens	13
17. Fresnel prism angle as a function of distance from lens axis	17
18. Image-forming lens	17
19. Fibers and configuration of fiber cone (a) entrance surface-hexagonal array configuration with $d = 25 \mu$, fiber size (b) exit surface-hexagonal array configuration with $d = 10 \mu$, fiber size and transmitted line pattern of ≈ 6 lines/mm	20
20. Fabricated fiber cone	21
21. Fabricated Fresnel lens	22
22. Fiber optical system assembly	22
23. Test equipment for system performance evaluations	23
24. Fiber cone with distortion corrector	24

ABSTRACT

The mechanics of light transmission through an optical dielectric cylinder have been known for some time, but only recently have advanced techniques in the fabrication of fiber optics allowed their application to the field of space. A fine fiber when surrounded by a coating of dielectric material of lower index of refraction transmits light energy by the mechanics of total internal reflection. Light rays propagate through the fiber by a series of reflections from wall to wall; and the fibers, when fused together to form a dielectric bundle, can convey an image. The bundle is capable of gathering a large quantity of light energy, since each fiber is, in essence, serving as an energy collector.

Light propagates through the bundle most effectively when the rays reach the entrance surface of the bundle at an incident angle equal to or less than the critical angle, which is primarily a function of the indexes of refraction of the core, the coating, and the surrounding media. To express the light-gathering power of the fiber, the term *numerical aperture* (NA) is used. (NA can be related to the *f*-number of a conventional lens system, to form a basis of comparison.)

As the light travels through the fiber, various losses of light energy occur. Since the overall transmission efficiency is affected by these losses, a clear understanding of the factors contributing to them is important in the study of fiber optics.

A theoretical analysis of fiber transmission efficiency was performed and the resulting data, computed by the IBM 7094 Computer, were utilized in the design of the fiber optical system. The quality of the transmitted image is primarily a function of the resolving power of the fiber optic. A theoretical analysis of the contrast and resolution characteristics of the fiber optics and the factors affecting image quality was also made.

A fiber bundle designed in the form of a cone with a larger diameter at the entrance than at the exit end will reduce an image size and permit the use of a conventional lens of longer focal length and larger

ABSTRACT (Cont'd)

effective aperture. Since there is a net gain in flux per unit area, this fiber cone can intensify as well as transmit an image. When coupled with a simple conventional lens, the cone and lens assembly are capable of high-speed, wide-angle applications.

To accept all the image light of the image-forming lens in an off-axis position, it is necessary for each fiber in the cone to accept light from all points of the lens aperture. For a lens having a relatively large field of view, a Fresnel lens is required to guide the extreme light rays into the fibers having a relatively smaller critical angle. An analysis of the Fresnel lens provided design equations. Various data computed by the IBM 7094 Computer were used to design the Fresnel lens.

Space environments impose severe constraints on the selection of material, component fabrication techniques, and mechanical design of the system, which must be capable of operating for prolonged periods in a space environment over a wide range of temperatures with a minimum degradation in performance. Accordingly, the properties of various materials were studied and suitable fabrication techniques were investigated. The mechanical design of the system took into consideration the minimization of system weight.

To verify the design as well as the system's capability, experiments and tests were performed utilizing the type approval requirements for space environmental testing per Jet Propulsion Laboratory Specification No. 30250. The fiber optical system was found to be suitable for space application. The incorporation of fiber optical elements makes it possible to simplify the design requirements and to realize a reduction in weight and volume without sacrificing reliability.

I. INTRODUCTION

A conventional lens system having a low f -number and a wide field of view contains many reflecting and refracting elements. Such a system therefore, poses problems in alignment and mechanical stability, especially when operating for prolonged periods in a space environment over a wide range of temperatures. Because of the large number of elements required, the dimensions of

such a system are relatively large and the weight is comparatively great.

A fiber optical system designed and constructed to overcome these difficulties is simple, rugged and capable of fast, high-resolution performance over a wide angular field.

II. FIBER OPTICS

The transmission of light through a transparent dielectric fiber by multiple internal reflection is a well known phenomenon. The fiber, when coated by dielectric material of lower refractive index, transmits light by total internal reflection occurring at the interface of the two media. A light ray propagates through the fiber by a series of reflections from wall to wall if the incident angle of the ray does not exceed the critical angle θ_c , given by

$$N_0 \sin \theta_c = (N_1^2 - N_2^2)^{1/2} f(\alpha, \psi, \beta) \quad (1)$$

where N_1 , N_2 and N_0 are the refractive indexes of the fiber core, coating, and medium surrounding the core and coating, respectively; and $f(\alpha, \psi, \beta)$ is a function of the position of the light source at the incident surface of the fiber and the ray direction. For the meridional case, $f(\alpha, \psi, \beta) = 1$, and Eq. (1) becomes

$$N_0 \sin \theta_c = (N_1^2 - N_2^2)^{1/2} \quad (2)$$

Light incident at an angle greater than θ_c will be reflected outside of the fiber rather than transmitted through it. When fused together to form a dielectric bundle, the fibers can be used to convey an image from one place to another.

A. General Characteristics

To express the light-gathering power of the fiber, it is convenient to refer to the term $N_0 \sin \theta_c$ in Eq. (2) as the NA of the fiber. Figure 1 shows the curves of the

NA as a function of N_1 and N_2 . By using glass with refraction indexes of 1.80 and 1.50 for the core and coating, respectively, it is possible to obtain a NA of 1. The light-gathering power of the fiber can be related to

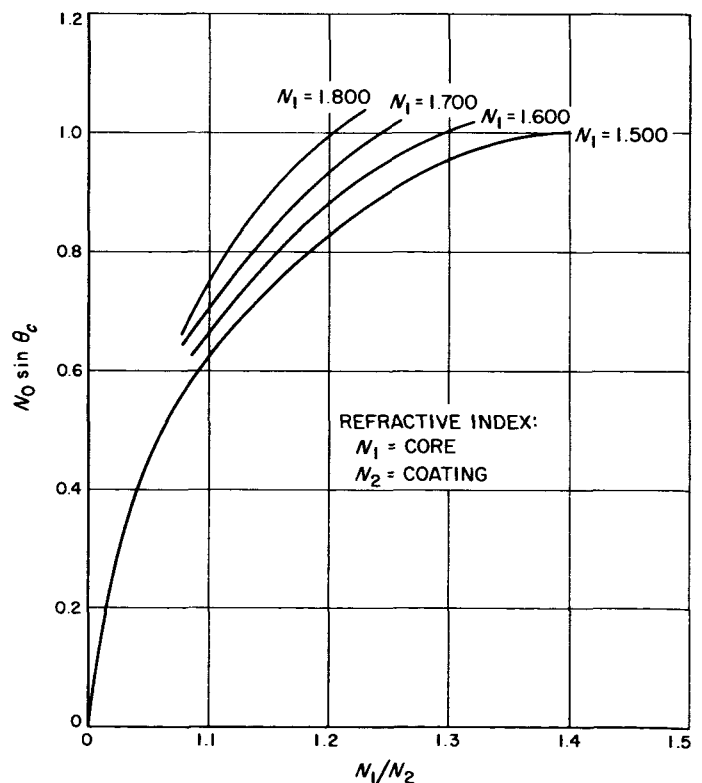


Fig. 1. Numerical aperture as a function of N_1/N_2

the equivalent lens speed of a conventional optical system by the relation (Ref. 1)

$$f = \frac{1}{2(\text{NA})} \quad (3)$$

where f is the ratio of the focal length to the effective aperture of the conventional lens. This comparison applies only when an image is already formed on the surface of the bundle and the fibers are used to transmit it from the entrance to the exit. The fiber optical bundle does not form images whereas a conventional lens does.

Two uncoated fibers with high indexes of refraction in direct contact with each other have a large reflection loss when the light strikes the interface. Energy leaks from one fiber to the other, degrading the transmitted image by causing loss of contrast and resolution. To preserve the characteristic of total internal reflection and to reduce the amount of leakage, the core is insulated with a coating that has a low index of reflection. To determine the effect of the coating on the transmission efficiency, the fraction of input energy transmitted can be calculated for an incident ray normal to the interface

$$R = \left(\frac{N_1 - N_2}{N_1 + N_2} \right)^2 \quad (4)$$

where N_1 and N_2 are the refraction indexes of the core and coating, and R is the fraction of the input energy reflected back to the core. The remainder of the input energy $(1 - R)$ is refracted into the coating and absorbed by it. It is seen from Eq. (4) that the transmission efficiency increases as the numerical value of N_2 decreases, and that the core must be surrounded by a coating with a lower index of refraction for optimum transmission.

In a multifiber bundle, the core area relative to the total area of the bundle is important from the standpoint of transmission efficiency. Since the coating does not convey useful information, it is desirable that the thickness be minimized. To establish a lower limit on the coating thickness, light transmission through the fiber bundle is expressed in terms of wave propagation. A light ray merely represents the direction along which the electromagnetic wave front is traveling. An analysis of the electromagnetic wave traveling through the fiber by total internal reflection indicates that the process of transmission is not as simple as that explained by the ray theory. According to the ray theory, the ray propagates through the fiber by a series of reflections at the interface between the core and the coating. According to wave theory, the electromagnetic wave actually pene-

trates the coating for some distance before reflecting back to the core. Moreover, the strength of the electromagnetic field of the wave decreases as it penetrates the coating. Analysis indicates that the field of the wave becomes negligible at a penetration of 1λ from the interface, where λ is the wavelength of the transmitted light (Ref. 2). Therefore, from a theoretical standpoint, it is reasonable to establish the minimum required coating thickness as 1λ .

When an image is formed upon one end of the bundle, the multiple reflections occurring within the individual fiber tend to integrate any variations in image intensity across its surface. Therefore, the intensity at the exit of the fiber appears uniformly bright. If the bundle is held stationary with respect to the image, the image is, in effect, sampled by the individual fibers, the sampling interval, and hence the resolving power of the bundle, being determined by the size of the fibers. Sampling theory states that if the information transmitted contains no frequency component higher than L lines/mm, the information can be completely specified by the ordinates of a series of points $1/2L$ mm apart. Since each fiber corresponds to a sampling point, the sampling interval for a single layer of fiber is d , where d is the fiber diameter. Therefore, $L = 1/2d$ is the highest frequency that can be transmitted by the bundle.

Transmission cutoff frequency can be increased if the fibers are packed in a hexagonal configuration instead of a square array. The square array is produced by single layers of fiber aligned to form a perfect square, whereas the hexagonal array is formed by aligning alternate layers of fiber. The hexagonal configuration produces more sampling points per unit area. Its cutoff frequency, based on geometric considerations, is 1.15 times that of the square array, or $1/1.74d$. The hexagonal arrays may not be uniformly arranged in a bundle because of structural imperfections. It is therefore reasonable to expect that the resolution of such a bundle lies between $1/1.74d$ and $1/2d$ in lines per millimeter when d is expressed in millimeters. For high resolution, it is required that the individual fiber be as small as possible. In addition to the difficulty of fabricating small fibers, there are a number of other major factors which impose a practical lower limit on the fiber size.

1. The area efficiency and the transmission efficiency decrease with the fiber size. For a bundle with small fibers, the area of the coating which transmits no useful information becomes a considerable percentage of the total area. For example, the area occupied by the coating for a bundle containing $10\text{-}\mu$

fibers and 1- μ -thick coating is nearly 20% of the total area.

2. As the diameter of the fiber is reduced, more and more energy travels along the bundle outside of the fiber. The transmission through one fiber produces a reaction in the neighboring fiber which degrades the contrast of the transmitted image.
3. When the fiber diameter becomes less than a few wavelengths of the light transmitted, the conduction of light becomes similar to microwave transmission by waveguides (Ref. 3). The bundle will transmit only light of certain wavelengths and incident angles to produce various mode patterns. Depending on the size of the fiber, these mode patterns tend to blur together at the exit end of the bundle. When the diameter of the fiber becomes less than one wavelength, the bundle will transmit limited light to one incident angle to produce the pattern of one mode.

B. Analysis of Transmission Efficiency

On the basis of thermodynamic reasoning, no increase in photometric efficiency is achieved where light is transmitted through the fibers in spite of their great light-gathering power. In fact, since various losses occur as light is conducted along the fiber, factors that affect transmission efficiency are important in the performance evaluation of fiber optics. Figure 2 shows a cylindrical fiber of diameter d and length L representative of the many fibers fused together to form a cylindrical bundle. When a cone of light having a half-cone angle of θ strikes the fiber surface a portion of the incident ray passes through the surface at a refraction angle of θ' . As the ray travels through the fiber, it bounces from wall to wall and eventually exits through the end surface. The various losses that occur as the ray passes through the fiber are analyzed on the basis of meridional ray considerations.

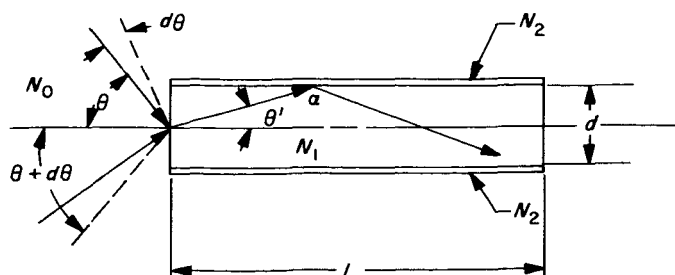


Fig. 2. Cylindrical fiber

The cone of light can be divided into three parts:

1. Part of the cone of light incident at the surface near the axis travels through the fiber without hitting the coating surface. The incident angle θ of this cone is

$$\theta = \sin^{-1} \frac{N_1}{N_0} \left[1 + \left(\frac{2L}{d} \right)^2 \right]^{-1/2} \quad (5)$$

2. The rays lying between θ and θ_c are conducted through the fiber and totally reflected at the cylindrical surface. The critical angle θ_c of the fiber was defined by Eq. (2):

$$\theta_c = \sin^{-1} \frac{(N_1^2 - N_2^2)^{1/2}}{N_0}$$

3. The rays lying outside the cone of incident angle θ_c are mostly refracted outside of the fiber and partially reflected at the surface. Energy conducted through by these rays is very small compared with the amount of energy transmitted by total internal reflection.

1. End Surface Reflection Losses

Energy is lost when the ray enters and leaves the bundle as a result of dielectric boundary reflection. This loss is a function of refraction indexes N_0 and N_1 of the two media and of the surface conditions of the fiber. If the fiber surface is assumed to be smooth and clean, the fractional loss due to surface reflection at the entrance is $R(\theta)$.

$$R(\theta) = \left[\frac{r_{\perp} + r_{\parallel}}{2} \right] \quad (6)$$

where r_{\perp} and r_{\parallel} are Fresnel coefficients of refraction for plane-polarized incident radiation when the E -vector of the electromagnetic wave is perpendicular and parallel, respectively, to the plane of incidence.

$$r_{\perp} = \frac{\left(\left(\frac{N_1}{N_0} \right)^2 \cos \theta - \left[\left(\frac{N_1}{N_0} \right)^2 - \sin^2 \theta \right]^{1/2} \right)^2}{\left(\left(\frac{N_1}{N_0} \right)^2 \cos \theta + \left[\left(\frac{N_1}{N_0} \right)^2 - \sin^2 \theta \right]^{1/2} \right)^2} \quad (7)$$

$$r_{\parallel} = \left\{ \frac{\cos \theta - \left[\left(\frac{N_1}{N_0} \right)^2 - \sin^2 \theta \right]^{\frac{1}{2}}}{\cos \theta + \left[\left(\frac{N_1}{N_0} \right)^2 - \sin^2 \theta \right]^{\frac{1}{2}}} \right\}^2 \quad (8)$$

where $R(\theta)$ of Eq. (6) is the Fresnel coefficient of refraction for unpolarized incident radiation. The fraction of energy refracted through the entrance surface is therefore $[1-R(\theta)]$. The fraction of energy leaving the exit surface after a second refraction is proportional to $[1-R(\theta)]^2$. The numerical values of $R(\theta)$ have been calculated in Ref. 4, and $[1-R(\theta)]^2$ is plotted as a function of θ for various values of N_1/N_0 in Fig. 3. It is noted that the transmission efficiency is fairly constant at incident angles $\theta \leq 50$ deg and decreases very rapidly at $\theta > 50$ deg. This is to be expected, since very little energy is transmitted by the rays reaching the surface at incident angles greater than the critical angle.

2. Absorption Loss

For a ray traveling through the fiber by a series of internal reflections, the length of the ray path $P(\theta)$ through a fiber having length L is

$$P(\theta) = \frac{L}{\left[1 - \left(\frac{\sin \theta}{N_1} \right)^2 \right]^{\frac{1}{2}}}$$

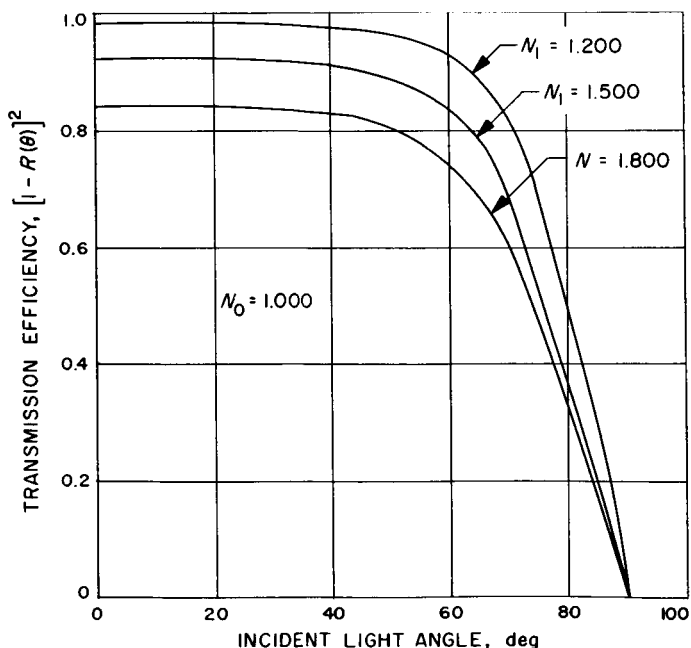


Fig. 3. Transmission efficiency as a function of incident light angle due to surface-reflection losses

Energy is lost along the path by glass absorption. As the length of the ray path increases, the fractional transmitted energy decreases exponentially.

$$\tau_A = \exp \left[\frac{-AL}{1 - \left(\frac{\sin \theta}{N_1} \right)^2} \right]^{\frac{1}{2}} \quad (9)$$

where A is the coefficient of absorption of the glass. To determine the effects of the various factors involved, the partial transmission efficiency τ_A as a function of AL and N_1 at the two limiting cases of $\theta = 0$ and $\theta = 90$ deg is calculated and plotted in Fig. 4. It is seen from this Figure that the transmission efficiency drops off very rapidly as AL increases, indicating the desirability of fabricating long fibers from glass with a low coefficient of absorption to minimize loss. It is possible, under certain conditions, to select a glass with an absorption loss as low as 0.25%/in.

3. Internal Reflection Losses

In spite of a smooth interface between core and coating, energy is absorbed by the coating each time the ray is reflected. For a ray with an incident angle of θ , the number of internal reflections before the ray reaches the exit end can be calculated by the following equation

$$N(\theta) = \frac{L \tan \theta}{d}$$

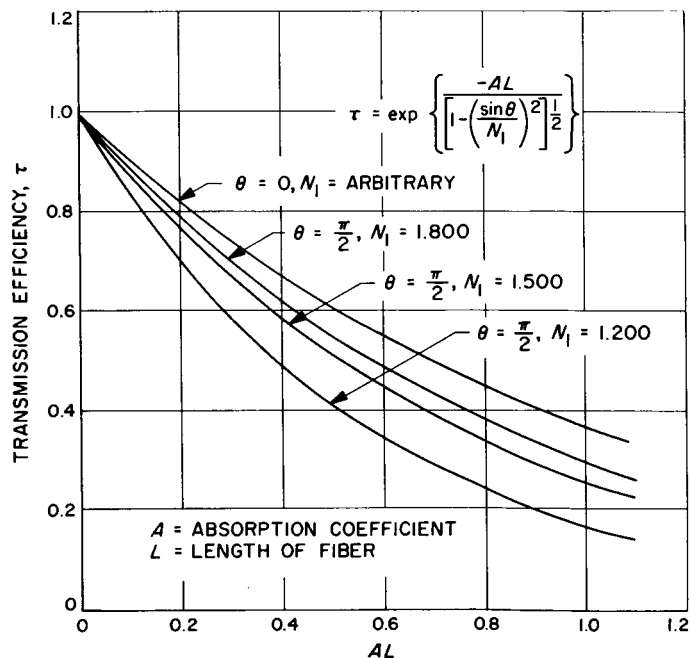


Fig. 4. Transmission efficiency as a function of AL due to glass-absorption loss

where θ' is the refraction angle. This angle can be related to the incident angle θ by Snell's law giving

$$N(\theta) = \frac{L}{d} \tan \left[\sin^{-1} \left(\frac{N_0}{N_1} \sin \theta \right) \right] \quad (10)$$

The fractional transmitted energy after $N(\theta)$ reflections is $[R_1(\theta)]^{N(\theta)}$. Here, $R_1(\theta)$ is the Fresnel coefficient of reflection for unpolarized light and can be evaluated by Eq. (6)–(8) with N_2/N_1 substituted for N_1/N_0 and α substituted for θ , where $\alpha = \frac{\pi}{2} - \theta'$.

$$\theta' = \sin^{-1} \left[\frac{N_0}{N_1} \sin \theta \right]$$

$$\alpha = \frac{\pi}{2} - \sin^{-1} \left[\frac{N_0}{N_1} \sin \theta \right]$$

It should be noted that the above analysis does not include the effect of the multipath reflections between the interfaces of the core and coating and the neighboring core and coating. It will be shown later that the magnitude of these higher-order reflections is generally small and can be neglected.

4. Total Transmission Efficiency

To derive a transmission efficiency equation with the losses taken into consideration, it is convenient to consider the incident energy contained in a hollow cone between θ and $d\theta$, as shown in Fig. 2. This energy is equal to the solid angle times the energy per steradian, or

$$dE(\theta) = 2\pi I(\theta) \sin \theta d\theta$$

where $I(\theta)$ is the energy distribution of the incident rays as a function of the incident angle θ .

where τ is the total transmission efficiency, τ_1 is the composite transmission efficiency including the various losses, and θ_0 is the half-cone angle of the incident light. To study the effects of the various parameters on the total transmission efficiency, Eq. (11) was solved by the IBM 7094 Computer using numerical integration for a number of cases. In the computation, the incident flux was assumed to be uniform [$I(\theta) = \text{constant}$], A was chosen to be 1%/in., and N_0 was set to 1.00 (for vacuum operation). The results are presented as curves in Fig. 5–9.

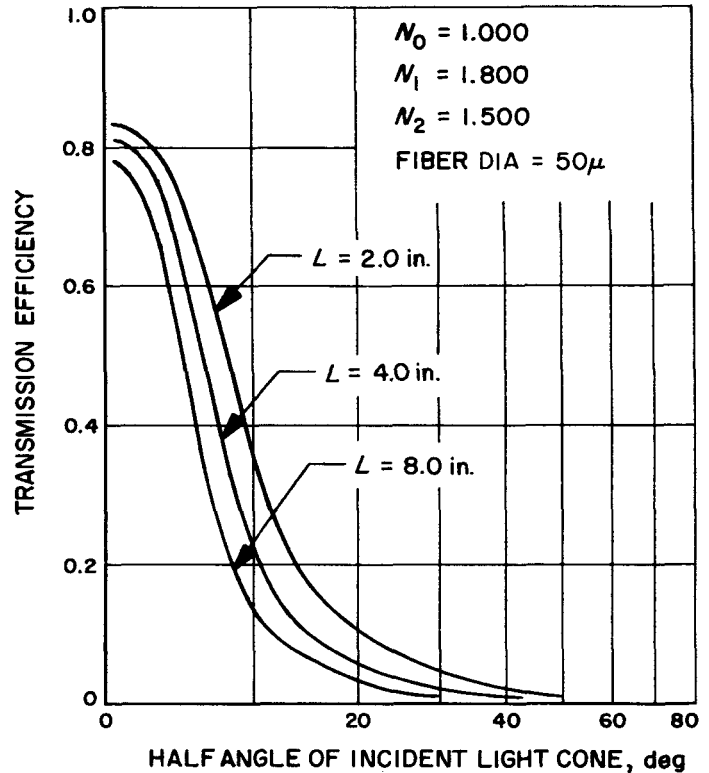


Fig. 5. Transmission efficiency as a function of half angle of incident light cone for $d = 10 \mu$

$$\tau = \frac{E(\theta)_{in}}{E(\theta)_{out}} = \frac{\int_0^{\theta_0} 2\pi I(\theta) \tau_1 \sin \theta d\theta}{\int_0^{\theta_0} 2\pi I(\theta) \sin \theta d\theta} \quad (11)$$

$$\tau = \frac{\int_0^{\theta_0} I(\theta) [1 - R(\theta)]^2 [R_1(\theta)]^{N(\theta)} \exp \left[\frac{-AL}{1 - \left(\frac{\sin \theta'}{N_1} \right)^2} \right] \sin \theta d\theta}{\int_0^{\theta_0} I(\theta) \sin \theta d\theta}$$

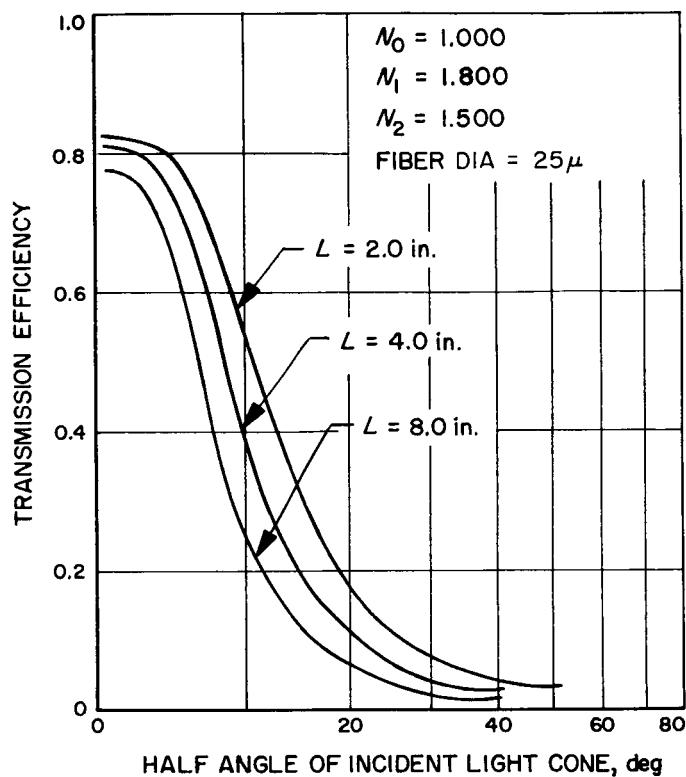


Fig. 6. Transmission efficiency as a function of half angle of incident light cone for $d = 25 \mu$

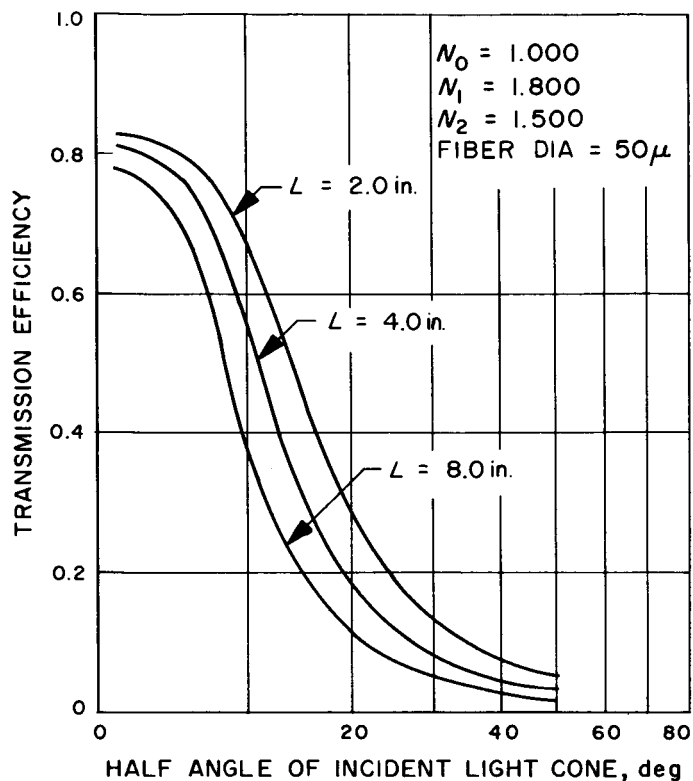


Fig. 7. Transmission efficiency as a function of half angle of incident light cone for $d = 50 \mu$

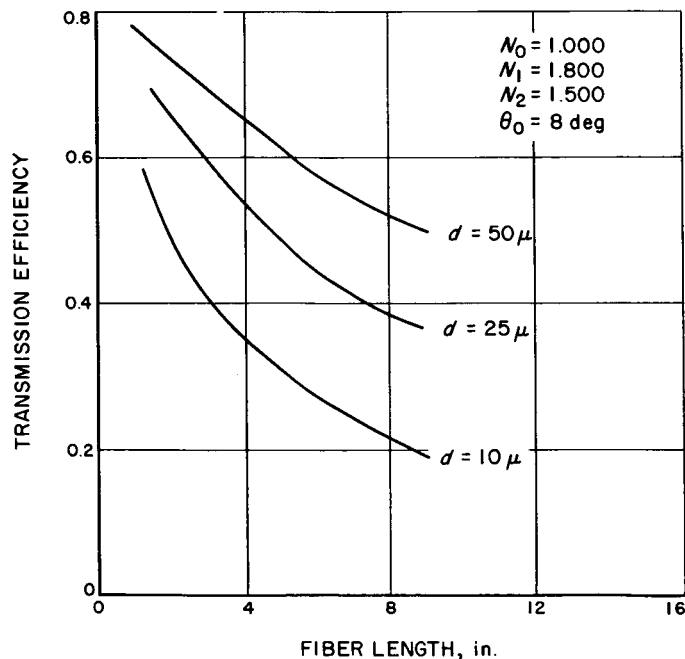


Fig. 8. Transmission efficiency as a function of fiber length

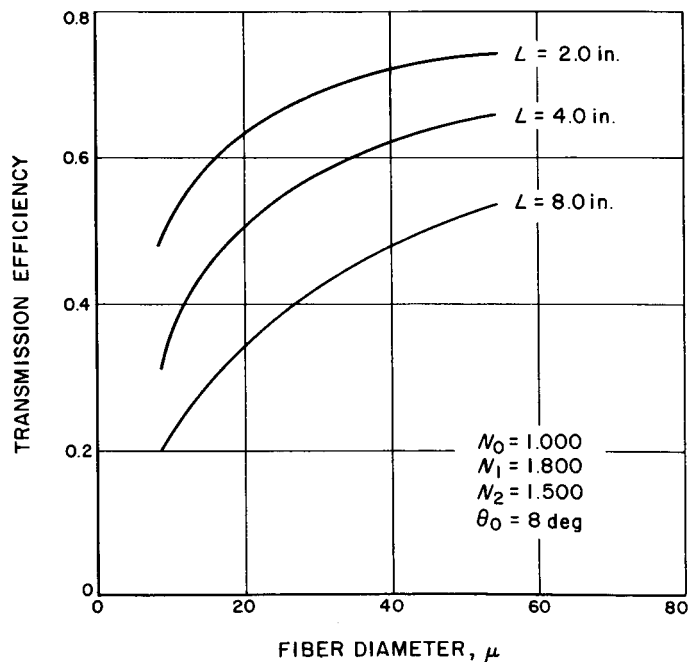


Fig. 9. Transmission efficiency as a function of fiber diameter

Figure 5 shows transmission efficiency as a function of the incident half-cone angle for bundles containing 10- μ fibers 2, 4, and 8 in. in length. Figures 6 and 7 illustrate transmission efficiency as a function of the incidence half-cone angle for fiber sizes of 25 and 50 μ , respectively, with the same fiber lengths. It is seen from these Figures that the transmission efficiency drops off very rapidly as the incident-light cone-angle increases. This is to be expected; as indicated in Section III, very little energy is transmitted through the bundle by light rays lying close to and outside of the critical angle. The energy transmitted per unit cone angle is small for these rays, and the average energy transmitted over the entire light cone decreases as the cone angle increases. Therefore, to obtain high efficiency, the light rays must travel as close to the bundle axis as possible. Figure 8 shows curves of transmission efficiency as a function of fiber length for fiber sizes of 10, 25, and 50 μ at a half-angle of the incident light cone of 8 deg. Transmission efficiency as a function of fiber diameter for 2, 4, and 8-in. fibers with an 8-deg half-angle of the incident light cone is presented in Fig. 9.

C. Analysis of Contrast and Resolution

The resolution of a fiber bundle is primarily a function of the fiber size and packing configuration: the smaller the fiber, the greater the resolution. However, there are factors limiting the size of the fiber, and these were discussed in Section II. It was determined that the resolution lies between $1/1.74 d$ and $1/2 d$ lines/mm for a hexagonal configuration when the fiber diameter is d mm. In that analysis, each fiber was assumed to be perfectly insulated from the neighboring fibers so that the light energy did not leak from one fiber to the other. During actual operation, however, a certain amount of energy does leak through the coating and penetrate the neighboring fibers. The cross-talk produced by this leakage degrades the image quality, contrast, and resolving power.

Figure 10(a)-(c) illustrates regions of leakage concentration. Figure 10(a) shows a fiber together with its six neighboring fibers in a hexagonal configuration. Obviously the leakage should be concentrated in the areas in which the fiber is closest to its neighbors (shaded areas in Fig. 10b). Light leakage outside these areas is small, since most of the energy is absorbed by the coating as it travels toward the neighboring core. In a hexagonal configuration, the six neighboring fibers are symmetrical with respect to the center fiber. Therefore, these leakage

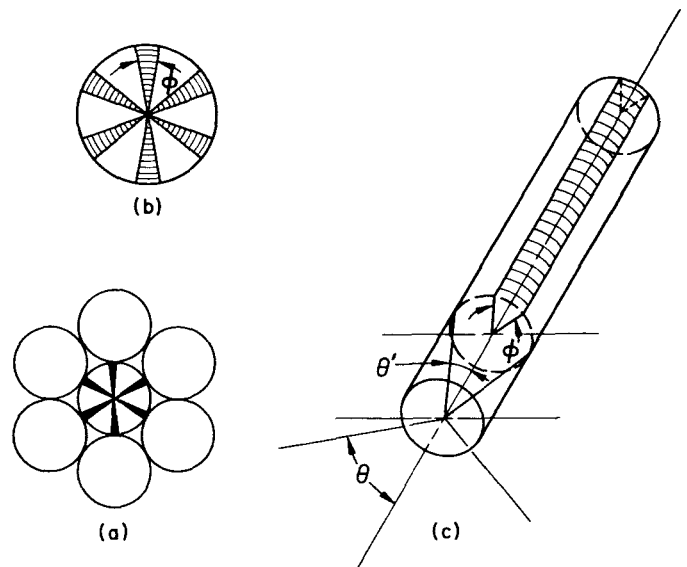


Fig. 10. Regions of leakage concentration

areas are located 60 deg apart, and the leakage characteristics of all areas are the same because of the symmetry. Figure 11 shows the center fiber with two neighboring fibers in a plane view.

Since a rigorous theoretical analysis of these leakages is very complicated, the following simplifying assumptions are made: (1) The thickness of the coating k is assumed to be small compared with the diameter of the fiber; thus, the absorption loss in the coating is negligible in the leakage area compared with the core absorption loss. (2) Higher-order multireflection of the refracted ray in the coating is neglected, since the energy refracted and reflected through two or more interfaces is generally small compared with that of the original refracted ray.

The path of a light ray after it reaches the entrance at an incident angle of θ is shown in Fig. 11. A portion

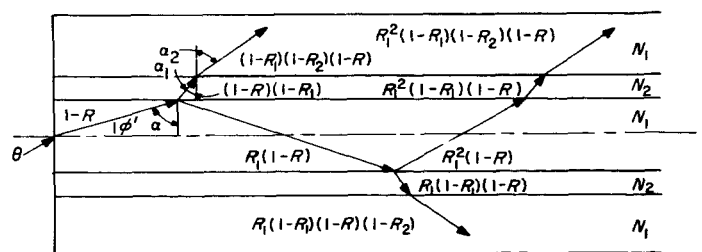


Fig. 11. Leakage due to internal reflection

of this ray, $[1 - R(\theta)]$, is refracted into the center fiber at an angle of θ' . When this refracted ray reaches the interface between the center core and coating, it divides into two components, $R_1(\theta)[1 - R(\theta)]$, which is reflected back to the center core, and $[1 - R_1(\theta)][1 - R(\theta)]$, which is refracted into the coating. Upon entering the neighboring core from the coating, a portion of the original incident ray has an amplitude of $[1 - R_2(\theta)][1 - R(\theta)][1 - R_1(\theta)]$ after the first internal reflection. This process is repeated as the ray bounces from wall to wall in the center core. The magnitude of the leakage to the neighboring core after N reflections can be calculated by summing the leakage components produced by each reflection. The fraction of light incident at the entrance of the center fiber which emerges from the exit of a neighboring fiber is

$$e(\theta) = \exp \frac{-AL}{\left[1 - \left(\frac{\sin \theta}{N_1}\right)^2\right]^{1/2}} [1 - R(\theta)]^2 [1 - R_2(\theta)]$$

$$[1 - R_1(\theta)] [R_1(\theta) + R_1(\theta)^2 + \dots + R_1(\theta)^{N(\theta)}]$$

$$e(\theta) = \exp \frac{-AL}{\left[1 - \left(\frac{\sin \theta}{N_1}\right)^2\right]^{1/2}} [1 - R(\theta)]^2$$

$$[1 - R_2(\theta)] R_1(\theta) [1 - R_1(\theta)^{N(\theta)}] \quad (12)$$

where $R(\theta)$ and $R_1(\theta)$ are the Fresnel coefficients of reflection of the fiber ends and the interface between the core and coating, respectively. These coefficients were defined in Eqs. (6)–(8). $R_2(\theta)$ is the coefficient of reflection of the interface between the neighboring core and coating:

$$R_2(\theta) = \frac{1}{2} [r_{2\perp} + r_{2\parallel}]$$

$$r_{2\perp} = \frac{\left\{ \left[1 - \left(\frac{N_1}{N_2} \right)^2 \sin^2 \theta' \right]^{1/2} - \frac{N_1}{N_2} (1 - \sin^2 \theta')^{1/2} \right\}^2}{\left\{ \left[1 - \left(\frac{N_1}{N_2} \right)^2 \sin^2 \theta' \right]^{1/2} + \frac{N_1}{N_2} (1 - \sin^2 \theta')^{1/2} \right\}^2}$$

$$r_{2\parallel} = \frac{\left\{ \left(\frac{N_1}{N_2} \right)^2 \left[1 - \left(\frac{N_1}{N_2} \right)^2 \sin^2 \theta' \right]^{1/2} - \frac{N_1}{N_2} (1 - \sin^2 \theta')^{1/2} \right\}^2}{\left\{ \left(\frac{N_1}{N_2} \right)^2 \left[1 - \left(\frac{N_1}{N_2} \right)^2 \sin^2 \theta' \right]^{1/2} + \frac{N_1}{N_2} (1 - \sin^2 \theta')^{1/2} \right\}^2}$$

$$\theta' = \sin^{-1} \left(\frac{N_0}{N_1} \sin \theta \right)$$

$$\exp \left\{ -AL / \left[1 - \left(\frac{\sin \theta}{N_1} \right)^2 \right]^{1/2} \right\}$$

is the fractional energy transmitted as a result of the glass absorption of the fiber. It should be noted that light leaks into a particular neighboring fiber occur only at the alternate reflections. However, it should also be noted that for every ray incident at angle θ , there is another ray incident at $-\theta$.

As shown in Fig. 10(b), there are six regions where the light transmitted through the center fiber leaks into neighboring fibers. One of the regions, which subtends an angle ϕ at the fiber axis, is shown in Fig. 10(c). Leakage angle ϕ , primarily a function of the fiber diameter and the wavelength of light being transmitted, can be evaluated by the following expression

$$\phi = 2 \cos^{-1} \frac{d - 2\lambda}{d}$$

where d is the diameter and λ is the wavelength.

The fraction of the energy incident at the center fiber which leaks through this region into any one of the neighboring fibers is

$$\tau = \frac{\frac{\phi}{2\pi} \int_0^{\theta_0} I(\theta) [1-R(\theta)]^2 [1-R_2(\theta)] R_1(\theta) [1-R_1(\theta)^{N_1(\theta)}] \exp \frac{-AL}{\sqrt{1 - \left(\frac{\sin \theta}{N_1}\right)^2}} \sin \theta d\theta}{\int_0^{\theta_0} I(\theta) \sin \theta d\theta} \quad (13)$$

To show the magnitude of this leakage as a function of the various parameters, Eq. (13) was solved by the IBM 7094 Computer by means of numerical integration for a number of cases. Again, the flux distribution as a function of θ is assumed to be constant ($I(\theta) = \text{constant}$), and A is chosen to be 1%/in. Light leakage as a function of the half-angle of the incident light cone for bundles with fiber sizes of 10 μ ; $N_0 = 1.00$, $N_1 = 1.80$, $N_2 = 1.50$; and fiber lengths of 2 and 8 in. is shown in Fig. 12. Leakage as a function of half-angle of the incident light cone for bundles with fiber sizes of 25 and 50 μ is shown in Fig. 13. It is seen from these curves that the leakage increases with half-cone angle. The rapid increase in leakage is due to the fact that most of the input energy incident at an angle equal to or greater than the critical angle penetrates the coating and leaks into the neighboring fiber. The effect of the leakage can be determined by examining the ratio of the energy transmitted through

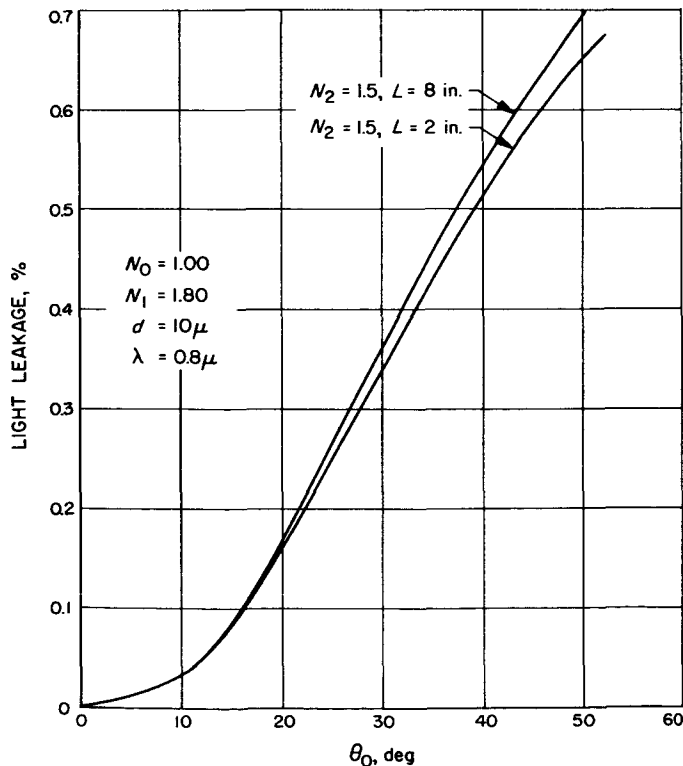


Fig. 12. Light leakage as a function of half angle of incident cone, $d = 10 \mu$

the center fiber to the leakage energy from the neighboring fiber. Energy transmitted by the center fiber for various cases is shown in Fig. 5-7; leakage from the neighboring fiber is shown in Fig. 12 and 13. Table 1 shows this ratio for fibers of various dimensions.

It is apparent that when fibers are insulated with a coating having a suitable index of refraction, the amount of leakage is small compared with the total energy

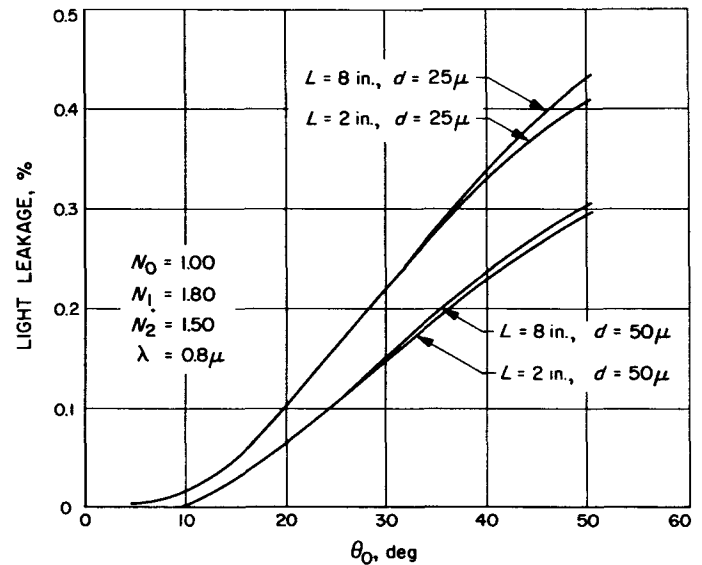


Fig. 13. Light leakage as a function of half angle of incident cone, $d = 25, 50 \mu$

Table 1. Ratio of transmitted energy to leakage energy for the primary refraction ray through fibers with $N_0 = 1.00$, $N_1 = 1.80$, $N_2 = 1.50$ and $\theta_0 = 8 \text{ deg}$

Bundle length, in.	Fiber diameter, μ	Transmitted energy / leakage energy
2	10	4500
2	25	18300
2	50	52300
8	10	1200
8	25	4500
8	50	12700

transmitted. The image quality is not seriously affected by the leakage as long as the ratio of the energy transmitted by the center fiber to the leakage from the neighboring fiber is greater than 50 to 1 (Ref. 2).

Since, Table 1 indicates, the leakage from the primary refraction ray is very small compared with the transmitted energy, that from the higher-order multireflected ray is negligible for all practical purposes and is, therefore, not considered in the analysis.

D. Analysis of Fiber Optical Cone

As discussed in Section II, a fiber optical bundle is capable of gathering a large amount of energy from an image formed at the entrance of the bundle. A fiber bundle can be fabricated in the form of a cone, with the diameter of the entrance larger than that of the exit. Such a cone is capable of both transmitting and intensifying an image incident at the entrance because there is a net gain in flux per unit area, the numerical value of which is primarily dependent on the ratio of the two end diameters and the transmission efficiency of the fiber cone. Since flux density is inversely proportional to image area, the photometric gain of a fiber cone (as in Fig. 14) is given by

$$g = \left(\frac{D_1}{D_2} \right)^2 \tau = \frac{1 - \cos \theta_1}{1 - \cos \theta} \tau \quad (14)$$

where D_1 and D_2 are the diameters of the entrance and exit, respectively, τ is the transmission efficiency of the cone, and θ_1 and θ are the exit and incident angles of a light ray. The NA, as defined by Eq. (2) for a cylin-

drical bundle, can now be modified for application to a fiber cone:

$$N_0 \sin \theta_c = N_1 \left[1 - \left(\frac{N_2}{N_1} \right)^2 \right]^{1/2} \frac{D_1}{D_2} \quad (15)$$

It is noted that the critical incident angle θ_c of the individual fiber is measured from the axis of that fiber. The angle $\theta_2(r)$ between the axis of the individual fiber and the axis of the cone depends upon the location of the fiber in the cone. If r is the distance from the cone axis to the axis of a particular fiber on the entrance surface, the critical angle $\theta_3(r)$ of that fiber with respect to the cone axis is

$$\theta_3(r) = \theta_c \pm \theta_2(r)$$

where

$$\theta_2(r) = \tan^{-1} \frac{1 - \frac{D_2}{D_1}}{L} r$$

$$\theta_c = \sin^{-1} \frac{N_1}{N_0} \left[1 - \left(\frac{N_2}{N_1} \right)^2 \right]^{1/2} \frac{D_2}{D_1}$$

The transmission efficiency equation derived for a cylindrical bundle can be utilized to estimate the cone efficiency by assuming that the fiber length L is equal to the average length of the axial and the outer fibers and that the fiber diameter is equal to the average diameter of the fiber at the entrance and exit surfaces.

As mentioned in Section II, fiber optics cannot form an image. In a conventional lens, the surfaces are curved and all rays reaching the lens are bent to meet at a point on the focal plane with the image being formed by the summation of all such points. For a fiber optic, no such ordered phase relationship exists; the image, therefore, must be applied to the entrance by an external lens system. Figure 15 shows a simple lens system, with the entrance surface of a fiber cone placed at the focal plane of the lens system. In order to accept all the image light in an off-axis position, each fiber must accept light from all points of the lens aperture. Since fibers will transmit light effectively only when the light ray has reached the surface at an incident angle smaller than the critical angle, each fiber must have a critical angle sufficiently large to accept light from all points of the lens aperture. This condition is difficult to fulfill for the outer fibers

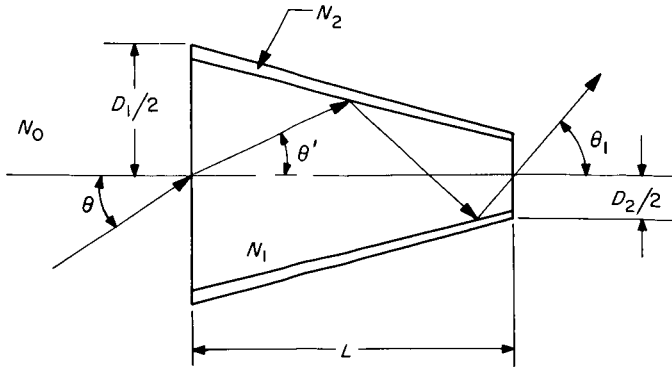


Fig. 14. Fiber optical cone

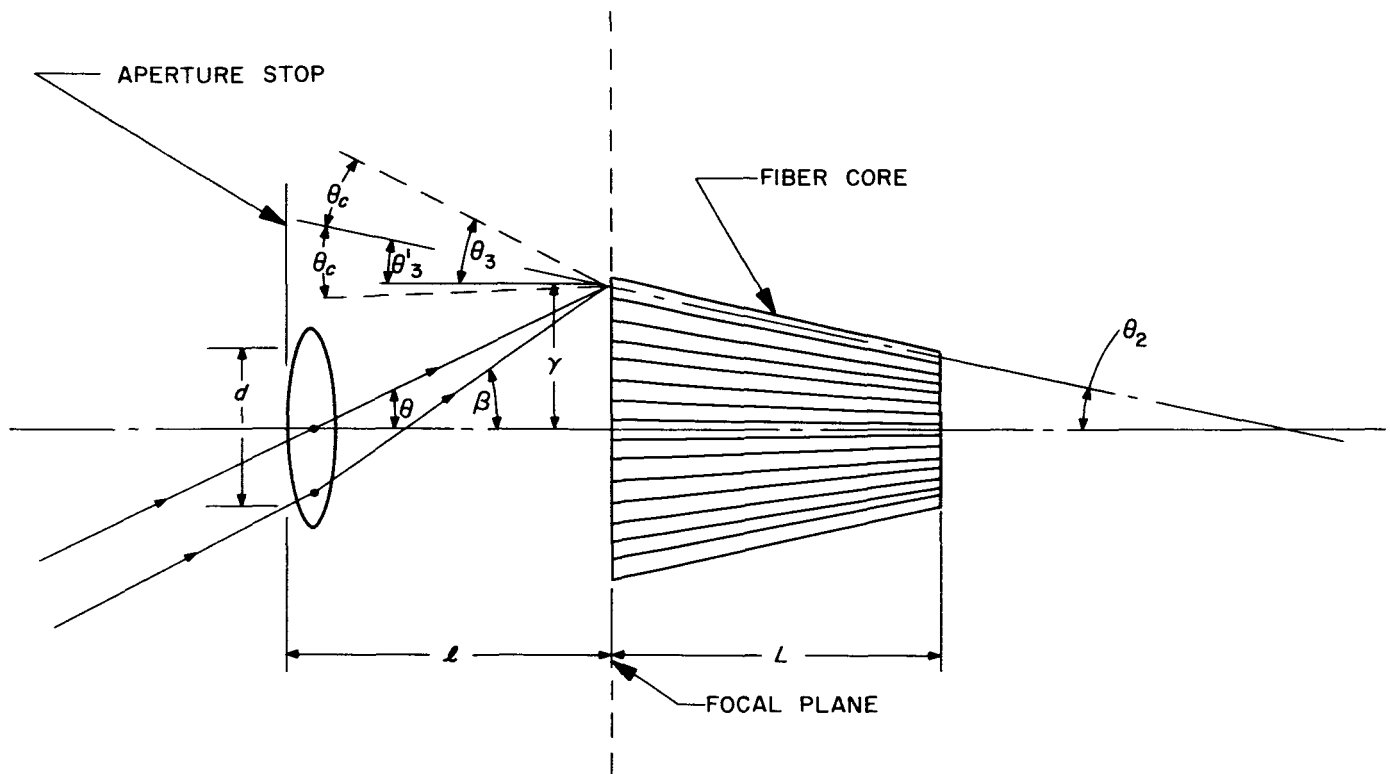


Fig. 15. Lens system and fiber cone

when the lens has a relatively large field of view, as shown in Fig. 15. Therefore, a corrective lens, such as a Fresnel lens, must be incorporated to guide the extreme light rays into an acceptable incident angle at the cone.

E. Application of Fresnel Lens

A typical Fresnel lens is shown in Fig. 16(a). It consists of a series of prism-like elements, each of which forms a zone of equal refraction. The Fresnel lens can

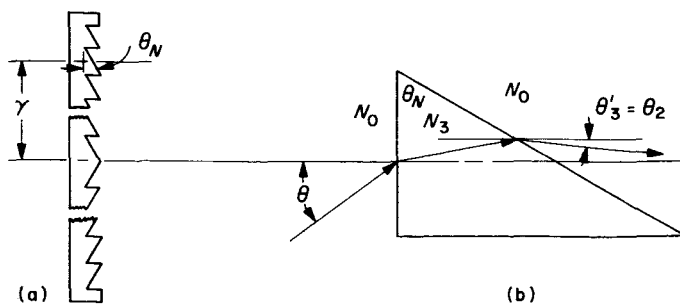


Fig. 16. Fresnel lens (a) the lens (b) an element of the lens

also be thought of as containing a series of concentric rings, each of which constitutes an equal refraction zone. Figure 16(b) shows an element of the lens. A ray reaching the entrance surface of the element at an incident angle of θ will pass through and refract out of the element at an exit angle of θ'_3 . With the value of θ held constant, the magnitude of θ'_3 is a function of θ_N , N_0 , and N_3 , where θ_N is the angle of the prism, and N_0 and N_3 are the refraction indexes of the surrounding medium and the prism, respectively. Therefore, it is possible to select the value of θ_N corresponding to a specific exit angle θ'_3 and incident angle θ by holding N_0 and N_3 constant.

A Fresnel lens can be utilized to divert the light rays within the field of view of the lens system into the critical angle of the individual fiber. With reference to Fig. 14 and 15, it is desired to bend the ray with an incident angle of θ into an angle θ'_3 , so that the bent ray will coincide with the axis of the fiber. Each fiber will be capable of accepting all the image light in an off-axis position if $\theta_c \geq \beta(0)$, where θ_c is the critical angle of the individual fiber and $\beta(0)$ is the angle of the off-axis ray at $r = 0$. To design a Fresnel lens for this application, the

following equation relating θ_N to θ and θ'_3 was derived:

$$\sin \theta = \frac{N_3}{N_0} \left\{ \sin \theta \left(1 - \left[\frac{N_0}{N_3} \sin (\theta_N + \theta'_3) \right]^2 \right)^{1/2} - \frac{N_0}{N_3} \cos \theta_N \sin (\theta_N + \theta'_3) \right\}$$

$$\sin \theta = \frac{N_3}{N_0} \sin \theta \left[1 - \left(\frac{N_0}{N_3} \right)^2 (\sin \theta \cos \theta'_3 + \cos \theta_N \sin \theta'_3)^2 - \cos \theta_N (\sin \theta_N \cos \theta'_3 + \cos \theta_N \sin \theta'_3) \right] \quad (16)$$

where

$$\tan \theta = \frac{r}{l} \quad (17)$$

$$\tan \theta'_3 = \frac{D_1 - D_2}{D_2 L} r \quad (18)$$

Equation (16) can be utilized to design the Fresnel lens. For a prism element located at a distance r from the axis of the lens, the numerical values of θ and θ'_3 can be calculated from Eq. (17) and (18) and substituted into Eq. (16), together with the proper values for N_0 and N_3 , to obtain the prism angle θ_N of the N th element at r .

III. FIBER OPTICAL SYSTEM DESIGN

A. Optical System Requirements

During the system design stage of a planetary scan system for a Mars mission, it was evident that an optical system of high performance was required to search for and track the planet. Based on the trajectory requirements and the expected amount of solar energy reflected from the planet and incident at the optics (Ref. 5), the following system constraints were established:

1. Angular field of view: 50 deg
2. Effective focal length: 10 mm
3. f -number: $f/1.0$
4. Frequency response: 0.5–1.1 μ , peak at 0.8 μ
5. Optical resolution: 20 line-pairs/mm
6. Image size: 0.5 in. max
7. Operating temperature: -40 to $+80^\circ\text{C}$
8. Weight: 1.25 lb max
9. Dimensions: 2.00 in. dia, 4.50 in. max length

Although it is possible to design and develop a conventional lens system capable of meeting the field-of-view and f -number requirements, such a lens is very complicated and requires a complex lens-element arrangement. Because of the large number of elements required, the dimension of the lens assembly would be relatively large and the final weight relatively high.

B. Design of Fiber Optical Cone

A fiber optical cone, coupled with a simple conventional lens system, is capable of both high-speed and wide-angle performance. The purpose of the fiber cone is to reduce the image size and to allow the use of a conventional lens of longer focal length and larger effective aperture. The combination of the fiber cone and conventional lens is capable of collecting large amounts of light, since the amount of light energy available to the detector is proportional to the effective area of the lens aperture.

To design the fiber cone, certain basic requirements must be established. The detector (Ref. 6) selected for the system is a p-n junction silicon device capable of generating a pair of output voltages V_x and V_y , proportional to the light spot-displacement X and Y on its surface. The output voltages of the detector are self-generating, and no bias voltage is required. The circular active surface area of this detector is 0.5 in. dia. The image-forming lens selected for the system is a standard commercial item, with a focal length of 30 mm and an f -number of $f/2.3$. This lens was selected for its light weight and small volume. For a field view of 50 deg, the image size for this lens is approximately 1.0 in. If the exit diameter of the fiber cone is chosen to be 0.5 in., the entrance diameter must be ≥ 1.0 in. to accommodate the full field of view of the lens.

The resolution of the fiber cone is dependent upon the fiber size. For a hexagonal configuration, the resolution L in lines/mm is

$$\frac{1}{1.74 d} \leq L \leq \frac{1}{2 d} \quad (19)$$

For a resolution requirement of 20 lines/mm, the fiber diameter at the entrance must be $25 = d \leq 28.7 \mu$, as calculated by Eq. (19). For an entrance fiber diameter of 25μ , an exit fiber diameter of 10μ , and an exit cone diameter of 0.5 in., the entrance cone diameter is determined to be 1.25 in.: $D_1 = 0.5 \left(\frac{25}{10} \right) = 1.25$ in.

To minimize weight it is desirable to make the cone as short as possible. The minimum length for a cone capable of accepting light reaching the entrance at an incident angle of θ_0 can be determined by

$$L_{\min} = \frac{\frac{1}{2} D_1 \left(1 - \frac{D_1}{D_2} \right) \cos \theta_0}{\left(\frac{D_2}{D_1} \right) \left[1 - \left(\frac{N_2}{N_1} \right)^2 \right]^{\frac{1}{2}} - \sin \theta_0} \quad (20)$$

where D_1 and D_2 are the cone diameters of the entrance and exit, respectively, and N_1 and N_2 are the refraction indexes of the core and coating. The operating condition of the optic determines θ_0 . At planet and spacecraft encounter, the apparent angular diameter of planet Mars is 15.4 deg when the spacecraft is on the nominal trajectory at 25,000 km from the planet. Therefore, the incident-light half-cone angle of 7.7 deg, or $\theta_0 \simeq 8$ deg, is utilized as a design objective. The light-gathering power of a fiber optic is proportional to its NA. To obtain a NA

of ~ 1 for a cylindrical bundle, or $1 \times D_1/D_2$ for the conical fiber, the numerical values of N_1 and N_2 can be calculated by means of Eq. (15). By assuming $N_0 = 1.00$ (for vacuum operation), N_1 and N_2 are found to be 1.80 and 1.50, respectively. All terms on the right side of Eq. (20) have been determined:

$$L_{\min} = \frac{\frac{1}{2} D_1 \left(1 - \frac{D_2}{D_1} \right) \cos \theta_0}{\frac{D_2}{D_1} \left[1 - \left(\frac{N_2}{N_1} \right)^2 \right]^{\frac{1}{2}} - \sin \theta_0}$$

$$L_{\min} = 1.20 \text{ in. for } D_1 = 1.25 \text{ in.}$$

$$D_2 = 0.50 \text{ in.}$$

$$N_1 = 1.80$$

$$N_2 = 1.50$$

$$\theta_0 = 8 \text{ deg}$$

Figure 8 can be used to estimate the transmission efficiency of the fiber cone by assuming that L is the average fiber length of the axial and outer fibers and d is the average diameter of the entrance and exit.

$$L = 1.225 \text{ in. for } D_1 = 1.25 \text{ in.}$$

$$D_2 = 0.50 \text{ in.}$$

$$L = 1.20 \text{ in.}$$

$$d = \frac{d_1 + d_2}{2}$$

$$d = 17.5 \mu \text{ for } d_1 = 25 \mu$$

$$d_2 = 10 \mu$$

The theoretical transmission efficiency, as shown in Fig. 8 for a bundle with $L = 1.225$ in. and $d = 17.5 \mu$, is 0.61, or 61%. The above calculation is based on the assumption that the cone is constructed entirely of conducting medium. However, the coating used in the cone cannot transmit useful information. For a closely packed hexagonal bundle, the ratio of the core area to the area of the bundle is given by

$$P = \frac{\pi}{3.464} \left(\frac{D}{D + d} \right)^2 \quad (21)$$

where P is the packing density and d and D are the diameters of the fiber and bundle, respectively. For $D = 1.25$ in. and $d = 25 \mu$ (or 9.84×10^{-4} in.), the packing density is 90% as calculated by Eq. (21). It should

be noted that P in Eq. (21) represents the packing density of a perfect bundle. Experience has indicated, however, that the packing density of actual bundles lies closer to 80% than to the theoretical value of 90%.

The photometric gain of the cone can now be evaluated by Eq. (14):

$$g = \left(\frac{D_1}{D_2} \right)^2 \tau P$$

$$g = 3.05 \text{ for } D_1 = 1.25 \text{ in.}$$

$$D_2 = 0.5 \text{ in.}$$

$$\tau = 0.61$$

$$P = 0.80$$

The conical fiber optic must be capable of transmitting energy in the visible spectrum as well as in the near-infrared region, from 0.5 to 1.1 μ as specified. Experiments indicated that most high-quality optical glass can transmit energy in these regions with negligible attenuation. Therefore, selection of the bulk material for the core can be limited to high-quality optical glass having the appropriate index of refraction.

The design requirements for the image-forming lens and the fiber cone can be summarized as follows:

1. Image-forming lens:

- a. Effective focal length: 30 mm
- b. f -number: $f/2.3$
- c. Circular field of view: 50 deg

2. Fiber cone:

- a. Refraction index of the core: 1.80
- b. Refraction index of the coating: 1.50
- c. Entrance diameter: 1.25 in.
- d. Exit diameter: 0.50 in.
- e. Entrance fiber diameter: 25 μ
- f. Exit fiber diameter: 10 μ
- g. Cone length: 1.20 in.
- h. Packing density: 80%
- i. Theoretical transmission efficiency: 61%

C. Design of Fresnel Lens

In order for the fiber cone to accept light from all points of the image-forming lens over the 50-deg field of view, a Fresnel lens is utilized to divert the off-axis light into the fibers.

Equations (16)–(18) can be used for the design of the Fresnel lens. Equation (16) is a transcendental equation relating θ , θ'_3 , θ_n , N_0 and N_3 . Angle θ can be calculated by Eq. (17) for each value of r , where r is the distance from the axis of the lens to the N th element of the lens. Equation (18) relates θ'_3 to r and the physical geometry of the fiber cone. It was mentioned in Section IV that the equations are valid if $\theta_c \geq \beta(0)$; θ_c can be calculated by means of Eq. (15).

$$\sin \theta_c = \frac{N_1}{N_0} \left[1 - \left(\frac{N_2}{N_1} \right)^2 \right]^{1/2} \left(\frac{D_2}{D_1} \right)$$

$$\theta_c = 23.6 \text{ deg for } N_0 = 1.00$$

$$N_1 = 1.80$$

$$N_2 = 1.50$$

$$D_1 = 1.25 \text{ in.}$$

$$D_2 = 0.5 \text{ in.}$$

From Fig. 16, $\beta(0)$ at $r = 0$ can be calculated by the simple geometric relation, $\tan \beta(0) = d/2l$, where d is the effective aperture and l is the focal length of the image-forming lens. Since the f -ratio is equal to the focal length divided by the effective aperture,

$$\tan \beta(0) = \frac{1}{2f}$$

$$\beta(0) = 12 \text{ deg, for } f = 2.3$$

From the above analysis, the numerical value of θ_c and $\beta(0)$ satisfy the condition of $\theta_c \geq \beta(0)$. Therefore, Eq. (16) can be utilized to design the Fresnel lens. θ_n , the prism angle of the N th element, in Eq. (16), was solved as a function of r and N_3/N_0 . These calculations were performed by the IBM 7094 Computer for a number of values of r . The results are plotted in Fig. 17.

Figure 17 indicates that the Fresnel prism angle increases with the distance from the lens axis. As expected, the rays reaching the image-forming lens at the extreme field of view require more correction. It is also noted that the higher the index of refraction of the Fresnel lens, the less correction is required. The Fresnel lens [Fig. 16(a)] consists of a number of prism elements, the quantity and physical size of which are determined by the size of the fibers at the entrance of the cone. It was decided that the size of elements should be 0.25 mm or

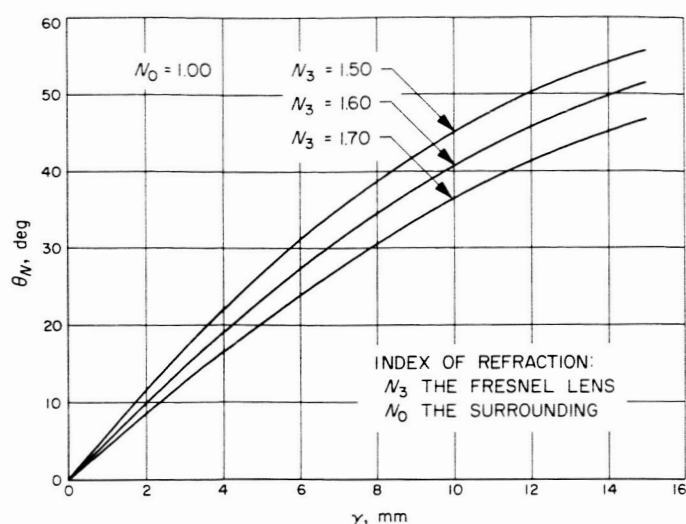


Fig. 17. Fresnel prism angle as a function of distance from lens axis

approximately 10 fibers per element. Experience indicates that very little improvement in performance will be obtained by decreasing the number of fibers per element for the application under consideration.

Transmission efficiency for a Fresnel lens is typically between 80 and 90%. The validity of these numbers can be demonstrated by assuming both surfaces of the lens to be parallel. The transmission loss is then primarily due to surface reflection and the fraction of the energy transmitted will be $[1 - R(\theta)]^2$ where $R(\theta)$ is defined by Eq. (6)–(8). It is seen, from curves of $[1 - R(\theta)]^2$ as a function of incident light angle θ on Fig. 3, that the transmission efficiency is fairly constant up to 50 deg. For $N_3 = 1.60$, the transmission efficiency is 82.5%. Therefore, it is reasonable to assume that the theoretical transmission efficiency of the Fresnel lens is on the order of 82.5%. The design requirements of the Fresnel lens can be summarized as follows:

1. Lens diameter: 1.25 in.
2. Index of refraction: 1.60
3. Number of elements: 120, or 100 elements/in.
4. Size of the elements: 0.25 mm or 1×10^{-3} in.
5. Element prism angle: As shown on Fig. 18

D. Design of Fiber Optical System

The fiber optical system consists of the fiber optical cone coupled with the image-forming lens. The Fresnel

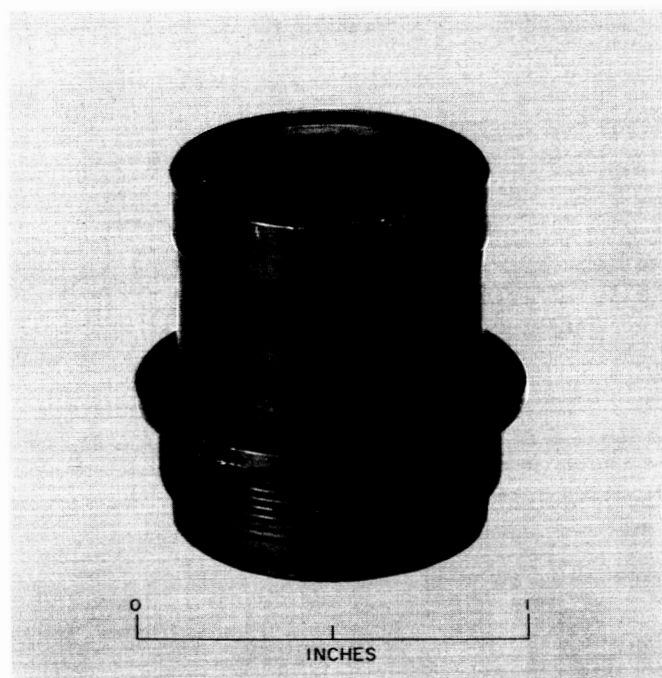


Fig. 18. Image-forming lens

correction lens is inserted between these elements and positioned on the image plane of the image-forming lens. The radiation detector is placed at the exit end of the fiber cone. To reduce reflection loss, an elastic optical coupling medium is utilized to couple the end surface of the cone to the detector. As the optic system is operating over a wide temperature range, the fiber cone, as well as the silicon detector, tend to expand and contract in accordance with the temperature gradient. Since glass and silicon have different temperature coefficients, the optical coupling medium will serve as a thermal shock absorber. Another purpose of the coupling medium is to serve as a mechanical shock absorber. These shock absorbing capabilities are necessary for space application.

The total transmission efficiency of the system is a function of the individual transmission characteristics of the image-forming lens, the Fresnel lens and the fiber cone. To derive a numerical value of system efficiency which can be utilized for comparison with a conventional lens, the transmission efficiency of the image-forming lens is assumed to be unity.

The transmission efficiency of the system is then $\tau = \tau_1 \cdot \tau_2 = (0.61)(0.825) = 0.503$ where τ_1 and τ_2 are the transmission efficiencies of the cone and Fresnel lens. An equivalent f -ratio of the system can be calculated by

the following equation

$$f_s = \frac{l_s f}{l \cdot (\tau)^{1/2}}$$

f_s = system f -number

l_s = system focal length

f = image-forming lens f -ratio

l = image-forming lens focal length

τ = system transmission efficiency

$$f_s = 1.08 \text{ for } l_s = 10 \text{ mm}$$

$$l = 30 \text{ mm}$$

$$f = 2.3$$

$$\tau = 50.3\%$$

The fiber optical system, when fabricated in accordance with the design data should have an f -ratio of 1.08, a figure slightly higher than 1.00 as specified by the system requirements.

The resolution of the system is primarily determined by the size of the fiber. The fiber cone was designed to have a resolution of 20 lines/mm, and it is reasonable to expect that the system resolution will be 20 lines/mm.

The frequency transmission of the system depends on the composite transmission characteristics of the individual components. As mentioned, the image-forming lens and fiber glass of high optical quality can transmit energy having a frequency range of 0.5–1.1 μ with little attenuation. Therefore, the frequency pass band of the system is primarily a function of the Fresnel lens. With a proper choice of material, the Fresnel lens is also capable of transmitting energy of the required bandwidth with little attenuation.

IV. FIBER OPTICAL SYSTEM FABRICATION

The effects of space environments impose severe requirements on the selection of material, component fabrication techniques and mechanical design. The system must be capable of operating for prolonged periods over a wide range of temperature with minimum degradation in performance. In addition, it must be capable of surviving the mechanical shocks and vibrations encountered during launch vehicle operation. The JPL Environmental Specification No. 30250 was used as a guide in the design and construction of the system.

A. Fabrication of Image-Forming Lens

The design of the system was such that a standard lens could be utilized to serve as the image-forming device. The lens selected is a standard commercial item having a focal length of 30 mm, field view of 50 deg and f -number of 2.3. This lens was selected because it is lightweight, small in volume and available as a standard item. Its resolution is 170 lines/mm on the axis and 80

lines/mm at the extreme field of view, which is considered adequate since the fiber cone is designed to have a resolution of only 20 lines/mm.

Being a standard commercial item, this lens is not designed mechanically for space application. Therefore, only the optical elements were acquired and these elements were then mounted in a metal housing. Because of the operating requirements, the material selected for this housing must in addition to the normal requirements for space applications have a: (1) thermal coefficient of expansion compatible with the optical element, (2) high strength-to-weight ratio, (3) minimum magnetic field. A logical choice would be a high-strength aluminum alloy such as alloy 6061T6 because of its low density and nonmagnetic property. An investigation, however, indicated that this alloy has a thermal coefficient of expansion of $24 \times 10^{-6}/^{\circ}\text{C}$ whereas that of the optical element is $9 \times 10^{-6}/^{\circ}\text{C}$. This large difference in thermal coefficients is undesirable in view of the wide operating temperature range. Stainless steel such as AISI 303 is

nonmagnetic, with a thermal coefficient of expansion of $14 \times 10^{-6}/^{\circ}\text{C}$. Although the weight of the lens assembly with the stainless steel mount will be higher than that with aluminum alloy, the gain in mechanical strength is worthy of consideration. The simplicity in the design of the optical elements enables the lens assembly to be compact in volume and the differential in weight will be small. Figure 18 shows the lens with a stainless steel housing.

B. Fabrication of Fiber Optical Cone

The glasses selected for the core and coating have indexes of refraction of 1.79 and 1.52, respectively. These values are considered compatible with the design requirements of 1.80 and 1.50 in view of the other requirements imposed on the selection. The fabrication technique requires that the melting point of the core material be higher than the melting point of the coating but that the core and coating material should have identical thermal coefficients of expansion. In addition, the glass selected must exhibit a minimum degradation in optical performance when exposed to the radiation of outer space for prolonged periods of time.

To fabricate the cone, fibers are drawn from molten glass of the core material. A coating is then placed on the individual fibers by inserting the core fiber in a tubing of molten coating glass, a technique similar to that described by H. S. Soutter (Ref. 7). A fine assembly of core and coating is then formed by pulling the core through a hollow cylindrical furnace. By controlling the amount of tension in the pulling, the diameter of the core and coating assembly is reduced to 850μ with a coating thickness of 40μ . Multiple fiber units are formed by placing the fibers in a hexagonal configuration and drawing them through a furnace at a temperature that will soften and fuse the coating together. The size of the individual fiber after this operation is reduced to approximately 50μ . These units are then combined to form a bundle. A mechanical jig is used to place the units in close contact with one another and to align them so that they all occupy the same corresponding positions at the two ends of the bundle. The entire assembly is then drawn through a furnace at a temperature sufficiently high to soften the coatings and fuse the units together. The pulling tension and the furnace outlet are adjusted to make the diameter of the fused bundle slightly larger than 1.25 in. The cone is then formed by pulling one end of the bundle through a furnace while holding the other end fixed. Finally, the tapered bundle is cut to the

proper length with the proper entrance and exit diameters and polished.

Experiments were performed to fabricate fiber cones by this technique. Many dead spots, produced by air trapped among the fibers during the bundle forming process, were observed in earlier cones. As the bundle was drawn to smaller size, the trapped air bubbles increased in size compared with the size of the drawn fiber. These dead spots were undesirable because of (1) reduction in transmission efficiency, (2) reduction in resolution, and (3) excessive thermal stresses on the fibers because of the difference in thermal coefficients of expansion of air and glass.

The above fabrication technique was then modified by drawing the bundle under vacuum. Cones having an entrance diameter of 1.25 in., fiber size of 25μ on the entrance end, and an entrance-to-exit diameter ratio of 2.5 were produced. Figures 19(a) and (b) show the fiber configuration of the entrance and exit surface. It is seen that although dead spots existed in the cone, the ratio of the dead spot area to the transmission area is small, and their effects are minor in this application. Figure 20 shows the fiber cone.

C. Fabrication of Fresnel Lens

Fresnel lenses can be fabricated by the standard techniques applicable to the construction of complex lens systems, i.e., by grinding and polishing the optical glass to form the lens. Because of the number of elements required on each lens, such a technique is too time consuming, especially when a number of lenses are required for preliminary design evaluations and hardware fabrication. An alternative method which overcomes this difficulty is to fabricate Fresnel lenses by the molding technique. A mold of proper design is constructed, and the lens is formed by molding an optical material. This method requires only one master mold per design. The optical material must be a compound having a moldable property similar to the polymers, be stable under vacuum and have the optical properties that will satisfy the design requirements.

It is well known that polymer compounds tend to lose weight in a vacuum due to sublimation and breakdown of the compounds. Extensive studies have been made on the behavior of the various compounds in space environment by JPL (Ref. 8) and by various space agencies (Ref. 9). The rate of weight loss, however, can be

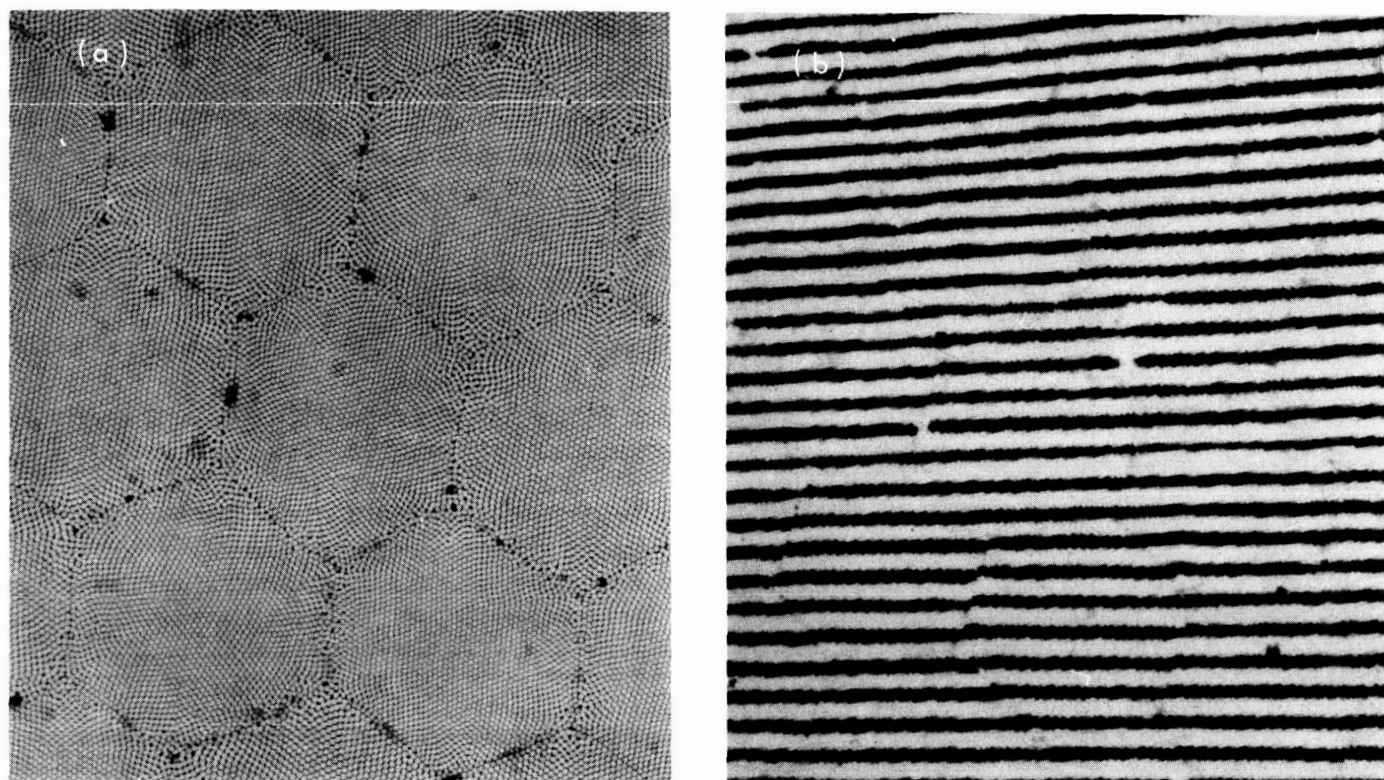


Fig. 19. Fibers and configuration of fiber cone (a) entrance surface-hexagonal array configuration with $d = 25 \mu$, fiber size (b) exit surface-hexagonal array configuration with $d = 10 \mu$, fiber size and transmitted line pattern of ≈ 6 lines/nm

kept to a minimum by the proper combination of chemical elements.

Preliminary investigation of a suitable material for this application indicated that a styrene copolymer possessed excellent molding and optical qualities. The important characteristics of the styrene copolymer, methyl methacrylate, are as follows:

Molding temperature	375°F
Tensile strength	9000 psi
Compression strength	13,000 psi
Impact strength	0.35 to 0.50 ft lb/in.
Thermal coefficient	$8 \times 10^{-5}/^{\circ}\text{C}$.
Index of refraction	1.533
Transmission	0.5 to 2.5μ
Weight loss rate	10%/yr at 350–400°F

The characteristics indicated that this compound is compatible with the mechanical and optical requirements of the system. The weight loss is specified at 10%/yr under vacuum conditions at a specific temperature range. This represents the upper limit of operating conditions without serious changes in its engineering properties. Since the maximum operating temperature for the system is anticipated to be 176°F (80°C), weight loss under these conditions will be considerably less than the value indicated. Investigation also indicated that this material possesses a fairly high degree of resistance to space and solar radiation damages. Figure 21 shows the Fresnel lens fabricated from this material.

D. Construction of Fiber Optical System

The design of the system is such that the image is formed at the surface of the Fresnel lens, for the purpose of the Fresnel lens is to divert the light rays having a wide field of view, into an acceptable cone angle at the fiber cone. The fiber cone transmits the incident ray at

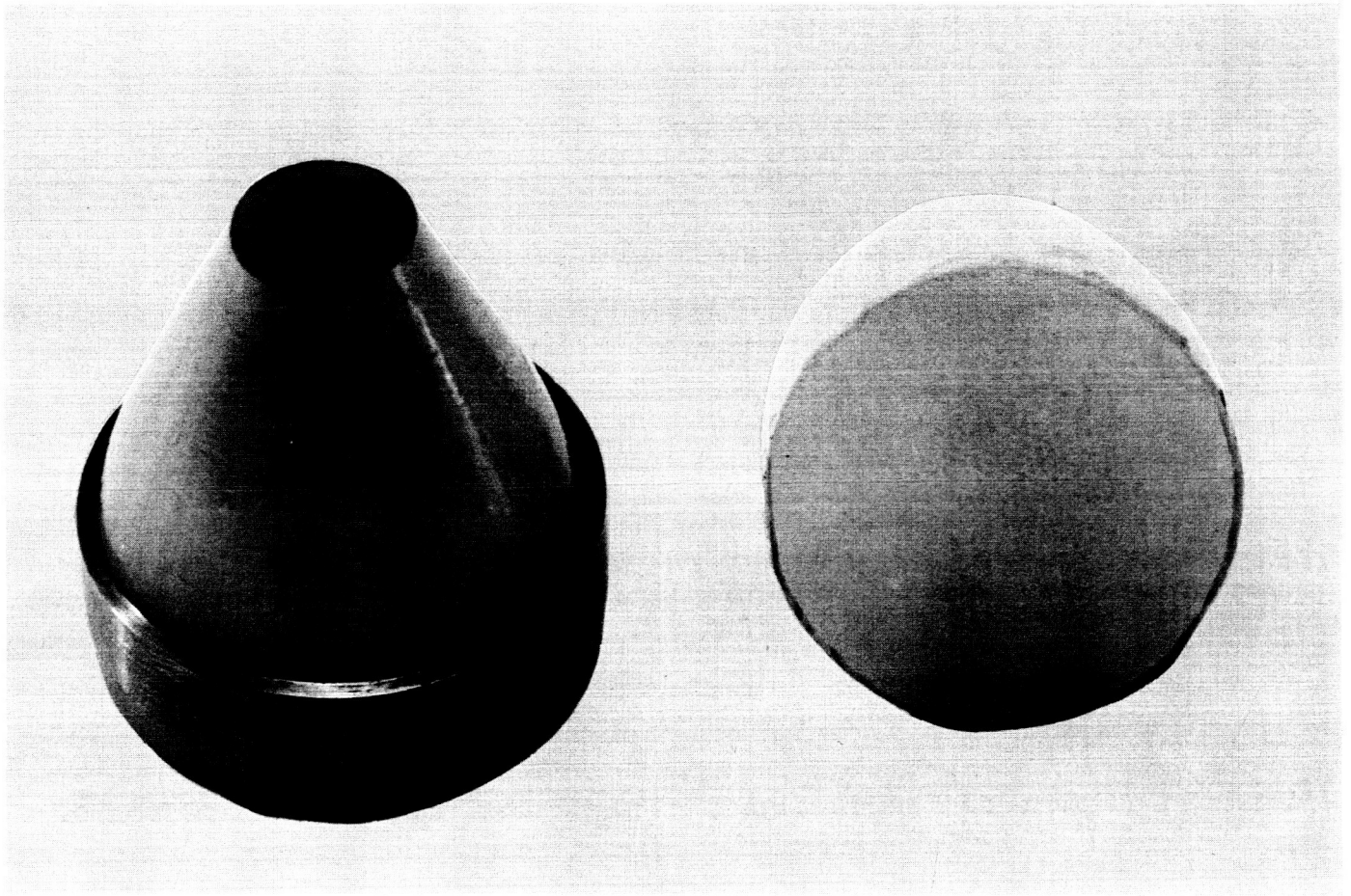


Fig. 20. Fabricated fiber cone

the entrance surface to form an image at the exit surface. To minimize reflection loss an optical coupling material, a silicone compound, LTV-306, manufactured by General Electric, is used to couple the exit surface of the cone to the detector. Because of its transparency, wide operating temperature range and low outgassing properties, LTV-306 has been used as an adhesive and coupling medium between solar cells and their protective covers on various space vehicles. The compound was applied between the fiber cone and the silicon detector with a thickness of 10 mils in order to provide mechanical and electrical shock absorption as well as optical coupling.

To conserve weight, the noncritical parts of the system such as the outer lens barrel, lens shade, detector hous-

ing and the system mount were fabricated from aluminum alloy 6061T6. Critical parts such as the lens mount and fiber cone mount were fabricated from stainless steel, AISI 303. A further reduction in weight was achieved by removing all excess metal which would not in any way weaken the structure. The total weight of the assembly, including the detector housing and mounting flange, was 1.20 lb. The optical system was 1.94 in. dia. and 4.0 in. in length and the detector housing measured $2.7 \times 2.7 \times 1.0$ in. The assembled system is shown in Fig. 22. It can be seen that there are provisions for mounting an electronic sub-unit on the back of the detector housing. All external surfaces of the system are gold plated to maintain the proper operating temperatures on a Mars trajectory by passive thermal control methods.

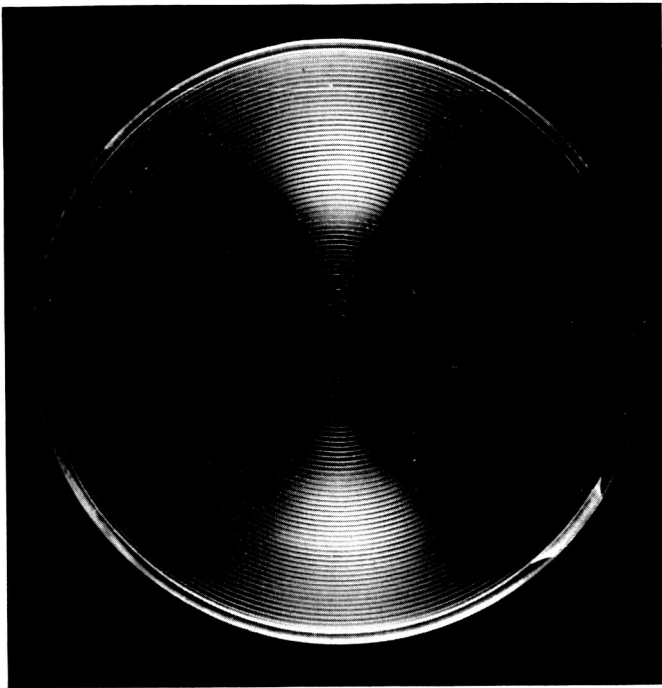


Fig. 21. Fabricated Fresnel lens

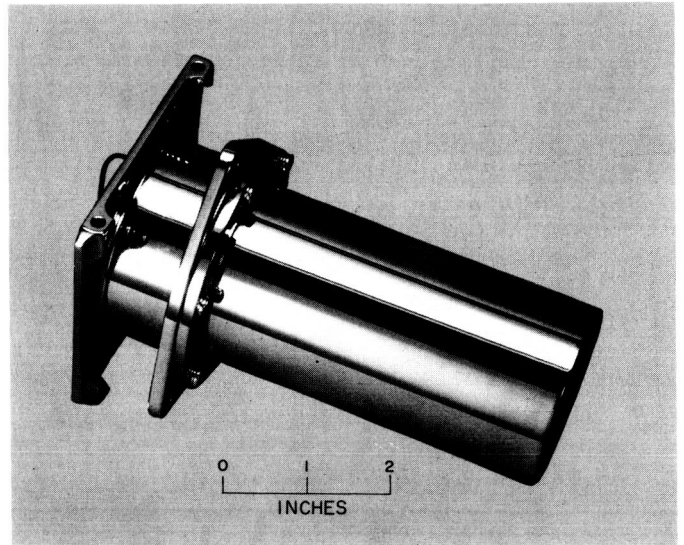


Fig. 22. Fiber optical system assembly

V. SYSTEM PERFORMANCE EVALUATION

The design of the fiber optical system was based on theoretical considerations. Whenever possible, components with proven levels of reliability were used; the selection of materials, fabrication and mechanical design were all oriented toward meeting the requirements of space environments. To verify the design as well as the system's capability the following experiments and tests were performed.

A. Image-Forming Lens Tests

The optical elements of standard design were mounted in a stainless steel housing and tested for optical performance and mechanical integrity under simulated space environment.

To determine the resolution of the lens, an NBS high contrast, 1952 target was placed 149 in. from the lens.

The image was formed on a Geatner microscope with an objective 10-power lens and a 6.7-power eyepiece. The horizontal and vertical resolutions were measured and calculated for on-axis and off-axis positions. On-axis resolution was approximately 170 lines/mm and off-axis approximately 80 lines/mm. An energy source with a known spectral distribution was used to determine the transmission characteristics of the lens. The spectral distribution of the source energy after it passed through the lens was measured, and very little attenuation was observed in the spectral range of 0.4–1.1 μ .

Shock and vibration tests in accordance with JPL Specification No. 30250 were performed on the lenses. Upon completion of these tests, the lenses were tested under thermal vacuum conditions in accordance with the same specification. The inspections and tests indicated that there was no apparent optical degradation or mechanical damage to the lenses.

B. Fiber Optical System Tests

A resolution check on the fiber cone and Fresnel lens was made by the use of the image-forming lens to form an image of the resolution target on the Fresnel lens together with the fiber cone. A microscope was used to observe the resolution of the assembly. The resolution of the assembly was approximately 20 lines/mm. A transmission characteristic test similar to the test performed on the image-forming lens was made on the assembly. Very little attenuation was observed in the spectral range of 0.5–1.1 μ . It was also observed that the glass of the fiber cone tends to absorb energy of wavelengths less than 0.5 μ . The theoretical spectrum of the reflected solar energy from the planet Mars (Ref. 5) shows that the contribution of energy at 0.5 μ or less is small compared to the total integrated energy. Therefore, the effect of attenuation of energy at 0.5 μ or less for this application is considered unimportant. It is also known that energy in the ultraviolet regions tends to degrade the performance of the silicon detectors. The absorption of energy by the fiber cone in the violet and ultraviolet has the

advantage of protecting the radiation detector and eliminating the need for a detector protective cover.

To determine the transmission efficiency of the fiber cone and Fresnel lens, a planetary simulator consisting of an illuminated disk 6 cm dia, an incandescent lamp source, filters and an iris diaphragm in a metal housing, (Fig. 23) was designed and constructed (Ref. 5). The transmission characteristics of the filters are such that only energy having a spectral distribution approximating the spectral reflectivity curve of the planet is allowed to reach the disk. An iris diaphragm is used to adjust the magnitude of the output energy without altering its spectrum.

The transmission efficiency of the fiber cone and Fresnel lens was determined by the use of the image-forming lens and radiation detector. The outputs of the detector were measured with and without the fiber cone and Fresnel lens in the system. Both measurements were made under the same input energy condition. The ratio of the two measured values determined the transmission

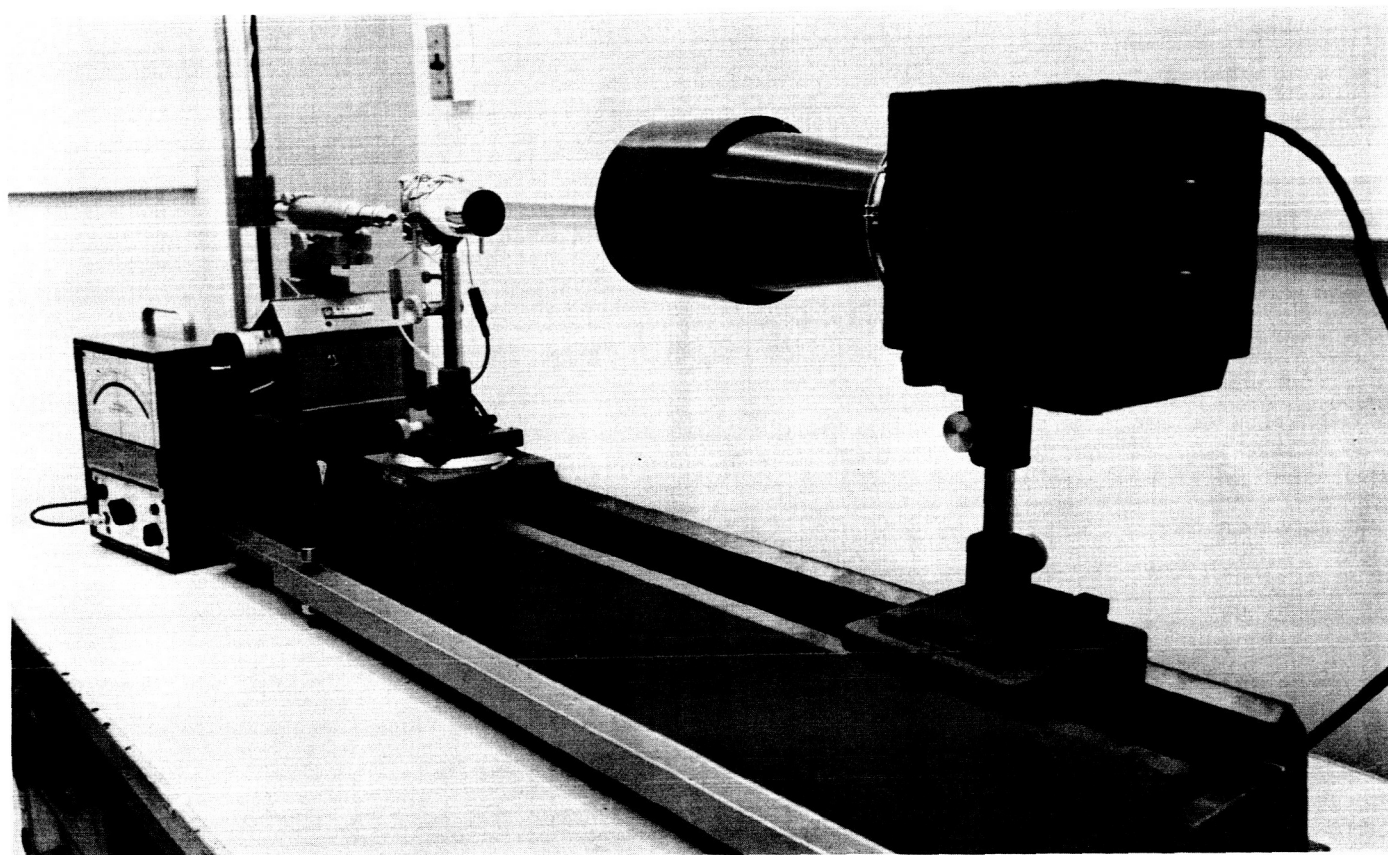


Fig. 23. Test equipment for system performance evaluations

efficiency of the fiber cone and Fresnel lens. Under the above testing conditions the measured transmission efficiency of approximately 48%. This value is lower than the calculated value of 50.3%. The difference possibly resulted from the fact that in the theoretical analysis, the fiber cone was assumed to be perfect and the interface between the core and coating perfectly smooth and clear. To account for the imperfection, the glass absorption loss in Eq. (9) can be modified:

$$\tau = (1 - k)^{N(\theta)} \exp \left\{ \frac{-AL}{\left[1 - \left(\frac{\sin \theta}{N_1} \right)^2 \right]^{1/2}} \right\}$$

where $N(\theta)$ is the number of internal reflections, $\exp \{ -AL/[1 - (\sin \theta/N_1)^2]^{1/2} \}$ is glass absorption loss and k is the reduction factor, the numerical value of which depended upon the physical conditions of the fiber optics.

Shock and vibration tests in accordance with type approval testing requirements of JPL Specification No. 30250 were performed on the fiber optical system. Again, the system was carefully inspected and optical tests were performed after these tests. Inspection and tests indicated that there was no degradation of the system.

VI. DISCUSSION AND CONCLUSIONS

The mechanics of light transmission through an optical dielectric cylinder have been well known for some time. Only recently has industry developed the techniques necessary to fabricate fiber optics capable of withstanding the severe space environment requirements. Theoretical analyses were made of light transmission through a fiber optic and the various factors affecting its performance. As a result, various data were computed and were, to a certain extent, verified by means of experiments. The results were used to serve as design data for the fiber optics system.

As previously mentioned, it is possible to design and construct a conventional optical system capable of meeting specific system requirements. The advantage of utilizing fiber optics is to simplify the design of the specified system and allow the use of a relatively simple, standard image-forming lens. The chief advantage of the fiber optical system, however, is its smaller weight and volume, two desirable features for applications where space and weight allocations are limited. As with the design and construction of many other types of flight equipment, the difficulty with the fiber optical system is the selection of materials. In addition to satisfying the optical design requirements, these materials, when operating together as a unit, must be capable of performing satisfactorily in space environments.

Since the system is designed to locate and track the planet at its bisector of brightness, the optical requirements are primarily dependent upon the amount of reflected solar energy available and the required tracking accuracy. From an optical standpoint, the system requirements are relatively loose in terms of resolution and distortion. The amount of distortion introduced by the use of the Fresnel lens, for example, would be intolerable for a system where a detailed study of the image is important. A fiber optic element, when properly designed and fabricated, is capable of correcting for field curvature and distortions. Figure 24 shows the fiber cone

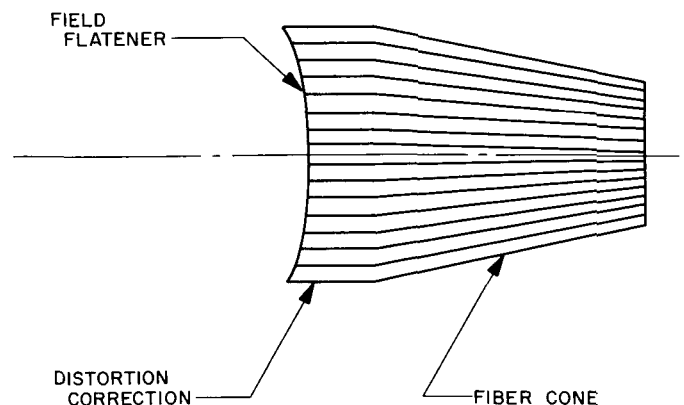


Fig. 24. Fiber cone with distortion corrector

modified to incorporate a distortion corrector. The fabrication of such a distortion-corrected fiber cone is complicated and much research and development is required before the proper fabrication techniques can be achieved.

This Report described the incorporation of a fiber optical element in an optical system for space application. Two other optical systems, the performance of which can be improved by the incorporation of fiber optical elements, are worthy of consideration. Photographic techniques for recording information displayed on a cathode ray tube suffer light and resolution losses because of light scattering through 2π steradians. A cathode ray faceplate can be made of fiber optical material with the phosphor applied directly to the inside face of the fiber plate. Pho-

tometric gain is possible from this arrangement by direct contact readout since each fiber of the faceplate is serving as a light collector. A second use for fiber optics arises from the fact that fiber bundles, when properly constructed, are flexible. Such a fiber bundle can transmit an image from one plane to another. The exit end of the bundle and the image readout device can be held stationary while the entrance end of the bundle is free to search for the objective over a wide angular area.

In this study, the characteristics of fiber optics have not been fully investigated. For the particular space application under consideration, however, the incorporation of fiber optics simplified the system design requirements. The advantages of reductions in weight and volume were realized to meet the system weight and volume allocated.

REFERENCES

1. Novatny, G. V., "Fiber Optics," *Electronics*, June 1962.
2. Kapany, N. S., "Image Quality and Optical Insulation," *Journal of the Optical Society of America*, August 1959.
3. Snitzer, E., and H. Osterberg, "Observed Dielectric Waveguide Modes in the Visible Spectrum," *Journal of the Optical Society of America*, May 1961.
4. Moon, P., "A Table of Fresnel Reflection," *Journal of Mathematics and Physics*, Vol. 19-20, 1940-41.
5. Jet Propulsion Laboratory, "Planetary Simulation for Mariner C Planetary Scan Subsystem," *Space Programs Summary 37-25*, Vol. II, Jet Propulsion Laboratory, Pasadena, November-December 1963.
6. Wong, R., "Analysis and Experimentations on Radiation Detectors," *Space Programs Summary 37-22*, Vol. IV, Jet Propulsion Laboratory, Pasadena, August 1963.
7. Soutter, H. S., *Proceedings of the Physical Society (London)*, 24, 166, 1912.
8. Jaffe, L. D., and J. B. Rittenhous, *Behavior of Materials in Space Environments*, Technical Report No. 32-150, Jet Propulsion Laboratory, Pasadena, November 1961.
9. R and D Technical Handbook, *Space/Aeronautics*, Vol. 40, No. 2, July 1963.

ACKNOWLEDGEMENT

The fiber optical system was developed and fabricated by Optics Technology, Inc., Belmont, California. The author wishes to express his appreciation to N. S. Kapany, D. F. Capello and C. Pernicone of Optics Technology, Inc., for their work on the fiber optical system and to D. W. Slaughter, F. L. Schutz and W. G. Fawcett of the Jet Propulsion Laboratory for their helpful suggestions.